

Institutionen för systemteknik

Department of Electrical Engineering

Examensarbete

Modeling of Engine and Driveline Related Disturbances on the Wheel Speed in Passenger Cars

Examensarbete utfört i Fordonssystem
vid Tekniska högskolan vid Linköpings universitet
av

Robert Johansson

LiTH-ISY-EX--12/4568--SE

Linköping 2012



Linköpings universitet
TEKNISKA HÖGSKOLAN

Modeling of Engine and Driveline Related Disturbances on the Wheel Speed in Passenger Cars

Examensarbete utfört i Fordonssystem
vid Tekniska högskolan i Linköping
av

Robert Johansson

LiTH-ISY-EX--12/4568--SE

Handledare: **M. Sc. Neda Nickmehr**
isy, Linköpings Universitet
Dr. Thomas Svantesson
NIRA Dynamics AB

Examinator: **Assoc. Prof. Lars Eriksson**
isy, Linköpings Universitet

Linköping, 1 June, 2012

	Avdelning, Institution Division, Department Division of Vehicular Systems Department of Electrical Engineering Linköpings universitet SE-581 83 Linköping, Sweden	Datum Date 2012-06-01
Språk Language <input type="checkbox"/> Svenska/Swedish <input checked="" type="checkbox"/> Engelska/English <input type="checkbox"/> _____	Rapporttyp Report category <input type="checkbox"/> Licentiatavhandling <input checked="" type="checkbox"/> Examensarbete <input type="checkbox"/> C-uppsats <input type="checkbox"/> D-uppsats <input type="checkbox"/> Övrig rapport <input type="checkbox"/> _____	ISBN _____ ISRN LiTH-ISY-EX--12/4568--SE Serietitel och serienummer ISSN Title of series, numbering _____
URL för elektronisk version http://www.vehicular.isy.liu.se http://www.ep.liu.se		
Titel Title Modeling of Engine and Driveline Related Disturbances on the Wheel Speed in Passenger Cars Författare Robert Johansson Author		
Sammanfattning Abstract <p>The aim of the thesis is to derive a mathematical model of the engine and driveline in a passenger car, capable of describing the wheel speed disturbances related to the engine and driveline. The thesis is conducted in order to improve the disturbance cancelation algorithm in the indirect tire pressure monitoring system, TPI developed by NIRA Dynamics AB.</p> <p>The model consists of two parts, the model of the engine and the model of the driveline. The engine model uses an analytical cylinder pressure model capable of describing petrol and diesel engines. The model is a function of the crank angle, manifold pressure, manifold temperature and spark timing. The output is the pressure in the cylinder. This pressure is then used to calculate the torque generated on the crankshaft when the pressure acts on the piston. This torque is then applied in the driveline model. Both a two wheel and a four wheel driveline model are presented and they consist of a series of masses and dampers connected to each other with stiff springs. The result is a 14 and 19 degrees of freedom system of differential equations respectively.</p> <p>The model is then validated using measurements collected at LiU during two experiments. Measurements were conducted of the cylinder pressure of a four cylinder petrol engine and on the wheel speed of two different cars when driven in a test rig. The validation against this data is satisfactory and the simulations and measurements show good correlation.</p> <p>The model is then finally used to examine wheels speed disturbance phenomenon discovered in the huge database of test drives available at NIRA Dynamics AB. The effects of the drivelines natural frequencies are investigated and so is the difference between the disturbances on the wheel speed for a petrol and diesel engine. The main reasons for the different disturbance levels on the front and rear wheels in a four wheel drive are also discussed.</p>		
Nyckelord Keywords Wheel speed disturbance, driveline model, engine model, torsional vibration, diesel engine, petrol engine		

Abstract

The aim of the thesis is to derive a mathematical model of the engine and driveline in a passenger car, capable of describing the wheel speed disturbances related to the engine and driveline. The thesis is conducted in order to improve the disturbance cancelation algorithm in the indirect tire pressure monitoring system, TPI developed by NIRA Dynamics AB.

The model consists of two parts, the model of the engine and the model of the driveline. The engine model uses an analytical cylinder pressure model capable of describing petrol and diesel engines. The model is a function of the crank angle, manifold pressure, manifold temperature and spark timing. The output is the pressure in the cylinder. This pressure is then used to calculate the torque generated on the crankshaft when the pressure acts on the piston. This torque is then applied in the driveline model. Both a two wheel and a four wheel driveline model are presented and they consist of a series of masses and dampers connected to each other with stiff springs. The result is a 14 and 19 degrees of freedom system of differential equations respectively.

The model is then validated using measurements collected at LiU during two experiments. Measurements were conducted of the cylinder pressure of a four cylinder petrol engine and on the wheel speed of two different cars when driven in a test rig. The validation against this data is satisfactory and the simulations and measurements show good correlation.

The model is then finally used to examine wheel speed disturbance phenomenon discovered in the huge database of test drives available at NIRA Dynamics AB. The effects of the drivelines natural frequencies are investigated and so is the difference between the disturbances on the wheel speed for a petrol and diesel engine. The main reasons for the different disturbance levels on the front and rear wheels in a four wheel drive are also discussed.

Acknowledgments

There are many people to whom I would like to express my gratitude. Without these people this thesis would not have been completed in such a manner as it is today. Firstly I would like to thank my supervisor at NIRA Dynamics AB, Thomas Svantesson and my university supervisor, Neda Nickmehr. They have offered invaluable support and assistance throughout the entire thesis. I would also express my gratitude to my examiner Lars Eriksson who has shed light on the subject of this thesis with his expertise and knowledge. I also would like to thank Peter Nyberg for his assistance during the experiments conducted on LiU. Finally I would like to thank all the other people at NIRA that have offered their assistance during my work, especially Predrag Pucar for letting me try to wreck his car and Daniel Mordin who has given me valuable and amusing lectures in the field of signal processing.

Contents

1	Introduction	1
1.1	Background	1
1.2	Objective and methodology	2
1.3	Outline	2
1.4	Previous works	3
1.4.1	Internal Combustion Engine (ICE) modeling	3
1.4.2	Driveline	4
1.4.3	Physical modeling in general	5
1.4.4	Tire pressure monitoring	5
2	System overview	7
2.1	Introduction	7
2.2	Powertrain	7
2.2.1	Engine	8
2.2.2	Driveline	9
2.3	Tire Pressure Indicator (TPI)	12
2.4	Desired output	12
2.5	Cylinder shutdown	14
2.6	Summary and concluding remarks	14
3	The internal combustion engine	15
3.1	Introduction	15
3.2	Four-stroke	15
3.3	Cylinder pressure model	16
3.3.1	Compression part	18
3.3.2	Determination of initial pressure and temperature	18
3.3.3	Expansion part	19
3.3.4	Flame characteristics and combustion phasing	20
3.3.5	Method to account for combustion phasing	21
3.3.6	Combustion part	22
3.3.7	Diesel engine parameterisation	22
3.4	Cylinder pressure torque	23
3.5	Summary and concluding remarks	24

4	Driveline	25
4.1	Introduction	25
4.2	Original two wheel drive model	25
4.3	Four wheel drive model	28
4.4	Front and rear system parameters	32
4.5	Gear dependency	33
4.6	Transferred torque and slip	34
4.6.1	Slip	35
4.7	Natural frequencies	36
4.8	Summary and concluding remarks	37
5	Validation	39
5.1	Measurements	39
5.1.1	Setup in the engine lab	39
5.1.2	Setup in the vehicle lab	39
5.1.3	Tests	40
5.2	Engine	42
5.2.1	Diesel engine model	47
5.3	Driveline	48
5.3.1	Error analysis	52
6	Results and conclusions	53
6.1	Results	53
6.1.1	Natural frequencies	53
6.1.2	Engine dependency	57
6.1.3	Front vs. rear wheel disturbances	62
7	Conclusions	65
7.1	Future work	66
	Bibliography	67
A	Notation	69
A.1	Variables and parameters	69
A.2	Acronyms	71
B	Cylinder volume	72

Chapter 1

Introduction

1.1 Background

A car driving with underinflated tires has higher fuel consumption and also an increased wear on the tires. For this reason an American law was formed in April 2005 stating that all new produced passenger cars with a weight below 3500 kg should have a Tire Pressure Monitoring System (TPMS). There are two ways of implementing tire pressure monitoring; direct and indirect. Direct tire pressure monitoring systems use pressure sensors in which the tire pressure is measured directly. This means however that the production cost for the car increases, due to sensor costs and installation. The other way of monitoring the tire pressure is to use the already existing sensors in the car, meaning wheel speed, ambient temperature etc. and applying sensor fusion to estimate the tire pressure. The indirect Tire Pressure Monitoring System (iTPMS) therefore comes with a lower cost than the direct pressure monitoring for the car manufacturer.

NIRA Dynamics AB is a company, founded in 2001, that has developed an iTPMS called Tire Pressure Indicator (TPI). TPI mainly uses the measurements from the wheel speed sensors to indicate deviations from the placard pressure. More specifically it looks at the relative change in the wheel speed signal and the spectral properties and how they change during a pressure loss. Disturbances also appear from the engine due to the ignition cycles and this disturbance spread through the driveline and are enhanced by the torsional effects. Under certain circumstances these disturbances from the engine are so large that TPI will have difficulties to determine the pressure situation in the tires. Such circumstances can be when driving at a specific engine speed torque ratio.

There are ways to suppress the disturbances coming from the driveline i.e. the components from the engine through the transmission and all the way to the wheels, but there is however an interest in finding out more about at which frequencies the disturbance appears and from where they originate. By achieving a sufficiently accurate model describing the engine torque fluctuation and its propagation through the transmission this can be achieved. An illustration of how the disturbances from the engine reach the TPI system is shown in Figure 1.1.

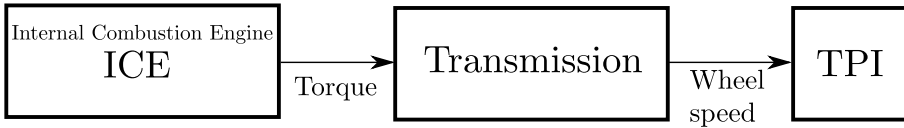


Figure 1.1. Diagram of how the disturbances originating from the engine reach the TPI system.

1.2 Objective and methodology

The goal of this thesis is to derive a model of the powertrain, i.e. the engine and driveline for describing the disturbances acting on the wheels. The model should be able to describe at which frequencies the disturbances appear and where they come from. This is to increase the understanding for this phenomenon in order to be able to suppress them more efficiently in the sensor fusion based TPI system. The model will be focused on cars with four stroke engines, manual gearbox and four wheel drive but should be as general as possible.

In the pre-modeling phase the model will be built and validated from already existing data provided from NIRA Dynamics AB; the data comes from real driving conditions and contains disturbances from the engine, as well as road irregularity and pressure related disturbances. When the model matches these measurements a car will be put into a test rig and isolated from the road so that only the information from the powertrain will appear. This data will then be used to further develop the model.

The model will then be used in order to explain and increase the understanding for some wheel speed disturbance phenomenon discovered in real car measurements.

1.3 Outline

This thesis consists of 6 chapters; where the first chapter consists of a brief introduction of the thesis and a literature review of what have been done so far associated to this work. In chapter 2 a brief overview is made over the different systems that this thesis covers. The different parts in an ordinary ICE and the driveline are explained. The wheel speed disturbance characteristics related to the drivetrain are explained and an introduction of the tire pressure monitoring system, TPI, developed by NIRA Dynamics AB is made. In chapter 3 the theory of a mathematical model for describing the output torque from ICEs will be explained. The model covers both petrol and diesel engines and consists of a cylinder pressure model and a model for calculating the crankshaft torque as a function of this pressure. Chapter 4 explains the theory of the used driveline model. The model is based on an existing two wheel drive model and is then further developed into a four wheel drive model. In chapter 5 the models from Chapters 3 and 4 are validated against measurements conducted at LiU. The measurements were made on the cylinder pressure on an Spark Ignited (SI) engine and the wheel

speed on two different cars that were mounted in a road simulation test rig. In chapter 6 the results of the thesis will be presented, some wheel speed disturbance phenomenon occurring in real cars are explained with the help of the complete powertrain model. The final chapter is chapter 7 which covers the conclusions made in the thesis and potential future works.

1.4 Previous works

There are many fields of research in which powertrain modeling plays an important role. The development of new engine control systems is one of them; the increased system complexity has led to an increased demand for physical engine models. Thus, models that can describe the complex cycle within the combustion chamber. Another area in which models of the powertrain is commonly used is in the investigation of the vehicle vibrations due to the torsional effects in the driveline. Even though the use of the powertrain model, derived in this thesis, differs from the ones which are described above the knowledge needed for modeling of the powertrain can be collected there.

Basic know-how in the field can also be acquired from several books written in the subject. One of them is [11] that covers the physics of the powertrain components and how to model and control these.

1.4.1 Internal Combustion Engine (ICE) modeling

Eriksson and Andersson in 2002, derived an analytic model that describes the cylinder pressure in a four stroke SI engine as a function of crank angle, manifold pressure, manifold temperature and spark timing [10]. The model describes the pressure during the expansion and compression phases as polytropic processes¹. It provides a convenient way of interpolation between these two phases to obtain the combustion pressure. The model is relatively easy to implement and fast to analyse, hence there is no need for a numerical solution of the ordinary differential equations.

In 2005 the model was implemented by Nayeri, with the purpose to simulate misfire. Even though the model never was validated, the report conclude that the model showed promising result regarding simulations of the cylinder pressure and misfire in the engine cylinders [16].

J. Scarpati et al. evaluated the ability of a studied engine model to predict engine noise in diesel engines for different control strategies. The model is based on [10] and the results are promising with high correlation between the model predictions and measurements made on an in-line 6-cylinder diesel engine [5].

Another work in which the model from [10] is used is [9], where the model is used to compare the combustion characteristics of gasoline and hydrogen fuelled spark ignited engines.

Another approach for deriving a model for the cylinder pressure is presented by Lim, et al., using the fluctuations in the crankshaft speed. The variations

¹See Section 3.3 for more information

in crankshaft speed origin from the ignition cycle and can therefore be used for backward calculations of the pressure in the cylinders [3]. As a pre-step in the derivation of the cylinder pressure, an expression of the torques provided from all cylinders in the engine is derived. For this thesis it would be a good idea to use this expression as an alternative instead of the pressure model, hence there is no actual need of knowing the cylinder pressure if you know the torque output.

In 1997 Rabeih did substantial research concerning models for the drivelines free and forced vibrations. More interesting for this thesis is that he gives a description of the engine torque as a function of cylinder pressure. He also describes a way of expressing the cylinder torque as a fourier-series in order to see how different torque excitations affect the torsional vibrations in the driveline.

F. Jones and C. Jezek, in 2008 used a series of thermodynamic differential equations to separately describe the pressure and temperature of the gases, liquids and mixtures in the engine cylinder. The model can simulate multiple injections and contains submodels describing the fuel spray, fuel evaporation and such. The model is partly validated and works seemingly satisfactory. The complexity of the model however makes it undesirable for this thesis, especially from a simulation time point of view [7].

In this thesis the cylinder pressure model derived by Eriksson and Andersson, [10] will be used in order to model the torque acting on the crankshaft. The model was chosen for its simplicity and the fact that it has been used with good results in other works, [16], [5]. The model will be used to simulate both diesel and petrol engines.

1.4.2 Driveline

When modeling how the engine torque propagates through the driveline, knowledge of the physical properties of the driveline components are needed. Eriksson and Nielsen give valuable tools for driveline modeling, with and without concern of the flexibility in the driveline axes as e.g. the propeller shaft, [11].

Rabeih in 1997, as mentioned above looked at vehicle vibrations originating from the driveline. He derives a complete damped torsional vibration model of the driveline system. The driveline components are well described and the methodology for calculating certain physical quantities, e.g. moment of inertia of the crankshaft are described, [20].

Nickmehr in 2011 investigated the drive quality in a passenger car as a function of free and forced vibrations due to torsional effects, and based her work on [20]. She models the driveline with respect to torsional effects excluding the engine. Instead she uses measurement data from cylinder pressure to calculate the driveline fluctuations. The resulting model is a system of differential equations (14-degrees of freedom) and an evaluation of solving strategies were done, [17].

A large amount of additional work has been done in the driveline modeling area with regard to torsional vibrations. Two of them are [2] who in 2010 derived a rear drive system model with focus on the differential gear, and [19] which derives a two wheel driveline model in order to identify disturbance phenomena in the driveline. The drawback of these models amongst others is that the crankshaft and cylinders

are to inadequately modeled to capture sub engine frequencies originating from the engine torsional fluctuations. Rabeih, [20] however uses a weak crankshaft model with the individual cylinder torque applied separately to obtain a model which can describe all the frequencies that the engine torque produces.

Petterson and Nielsen derive a driveline model in order to investigate how to construct an engine control strategy that dampens the effects of the driveline resonance phenomenon. This with respect to driver comfort and the time response of the car for a change in accelerator position. The model suffers from the same drawbacks as [2] and [19]; the effects that the resonance frequencies have on the wheel speed is however particularly interesting for this thesis, see [13].

This thesis will use the driveline model derived by Rabeih, [20] as a starting point and then further develop it into a four wheel driven driveline model. The model has an appropriate level of detail for this thesis and has successfully been used by others. The parameters used in the model are provided in [20], to have these parameters makes it easier to implement since these parameters are often hard to acquire.

1.4.3 Physical modeling in general

When it comes to solving the mathematical equations of the models e.g. state-space or Differential Algebraic Eqations (DAE), there is a wide range of methods to use. Ljung and Glad, [12], presents some of the most commonly used solving strategies in this field; other aspects helpful for this thesis are also described. This including general recomendations for physical modeling and an introduction of object oriented modeling using the programming language Modelica. Further mechanical modeling methods are described in [4], which when it comes to the mathematical modeling systematic it focuses on describing how to use the Bond-Graph method to model driveline components.

1.4.4 Tire pressure monitoring

Since the ultimate purpose of this thesis is to improve the indirect tire pressure monitoring system TPI, it is of utmost importance to have knowledge of the theory behind it. Several reports and articles are available on the subject. An introduction of the usage of the wheel speed signal for estimation certain wheel and tire related quantities is made in [6]. How to calculate the friction between the tire and the road, unbalance of the wheels and pressure loss detection are covered. Persson et al. looks more specific on tire pressure monitoring by using the wheel speed signal. The paper describes two ways for using the wheel speed signal for tire pressure monitoring, wheel radius analysis and vibration analysis. Wheel radius analysis calculates a relative wheel radius from the wheel speed signal and can therefore detect a pressure loss in 1-3 tires. In the vibration analysis changes in the resonance frequency of the tire that is excited by the road vibrations is used to indicate deviations from the placard pressure [15]. It is in the latter method that disturbances from the engine and driveline can cause problems. In [18] some implementing issues are discussed in order to enable these systems to be fitted into

an automotive micro processor, and there by commercialising the product.

Chapter 2

System overview

2.1 Introduction

In this chapter a brief overview is made over the different systems that the thesis cover. The different parts of an ordinary ICE and the driveline are explained. The powertrain related wheel speed disturbance characteristics are explained and an introduction of the indirect tire pressure monitoring system, TPI, developed by NIRA Dynamics AB is made. The following notations are used in the entire thesis; the term powertrain denotes the engine and the parts used to transmit the power out to the road, e.g. gearbox, propeller shaft and wheels. The term driveline is used to describe the powertrain without the engine.

2.2 Powertrain

In this section the main components of a powertrain are explained, this to increase the understanding for the model in the following chapters. The function of the powertrain is to produce and deliver mechanical energy to the wheels. In Figure 2.1 a front-engine four-wheel-drive vehicle powertrain is illustrated. The most common components of a powertrain are engine, flywheel, clutch, gearbox, propeller shaft and universal joints, differential, wheel axle assembly and tires.

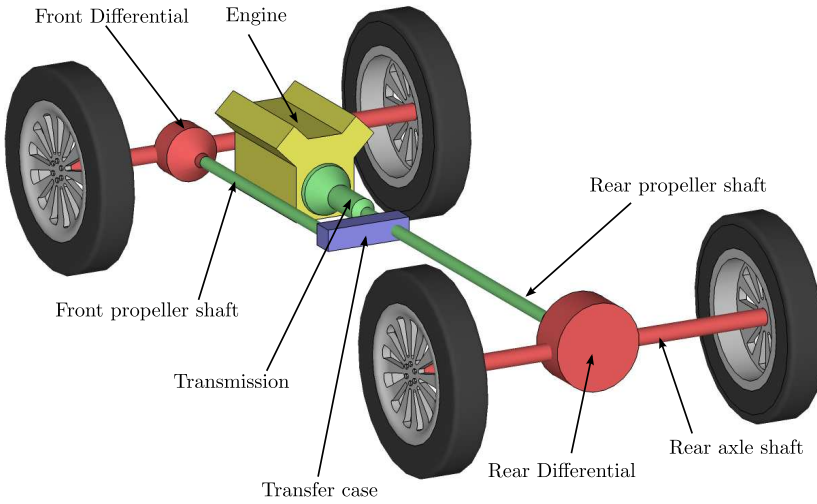


Figure 2.1. Front-engine four-wheel-drive vehicle powertrain.

2.2.1 Engine

The engine is the component producing power in the powertrain. The main components of the internal combustion engine are intake and exhaust valves, cylinder, piston, connecting rod and crankshaft which are shown in Figure 2.2. The engine produces power by sucking in fuel in to the cylinder that then ignites and creates a force on the piston. The piston then acts on the crankshaft creating a torque. In Figure 2.3 an illustration of four pistons mounted on a crankshaft is shown.

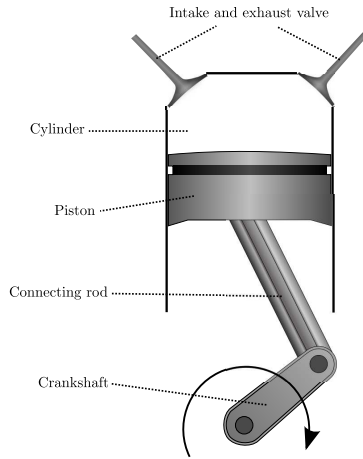


Figure 2.2. Main engine parts.

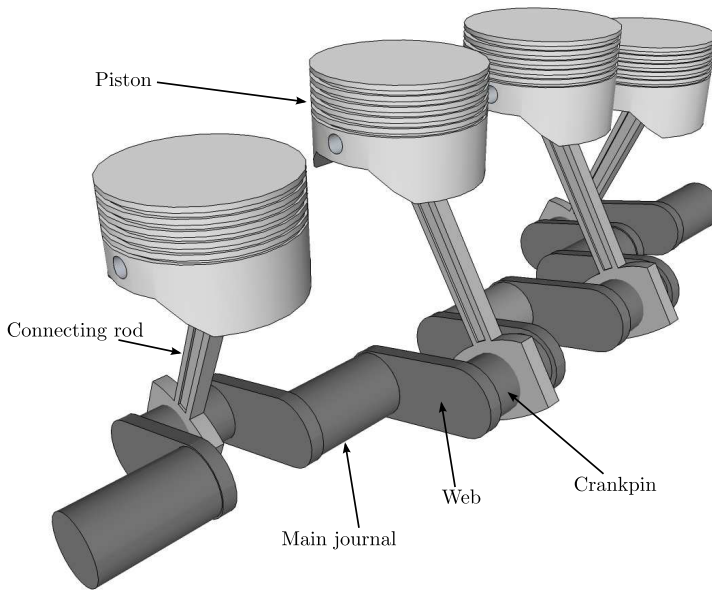


Figure 2.3. Four pistons mounted on a crankshaft.

2.2.2 Driveline

The purpose of the driveline is primarily to deliver the power produced in the engine to the wheels. The main components of an ordinary driveline is schematically

illustrated in Figure 2.4 and a brief description of each component follows below.

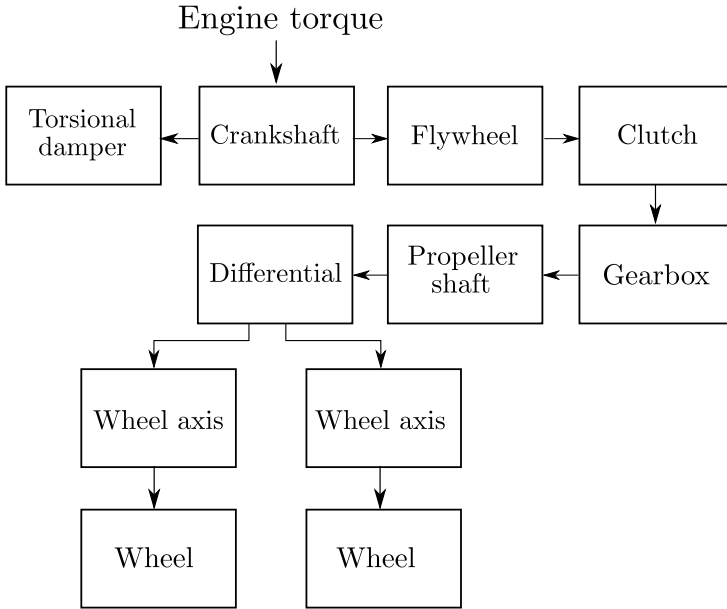


Figure 2.4. Schematic view of the main driveline components.

Torsional damper: The torsional damper is basically a mass attached to the front of the crankshaft, this in order to decrease the acceleration of the crankshaft when the engine ignites and to balance the entire engine assembly.

Crankshaft: As previously mentioned the crankshaft is the shaft on which the engine torque is applied and this creates the rotating motion of the engine.

Flywheel: On the crankshaft a flywheel is mounted. A flywheel is a rotating mechanical device that is used to store rotational energy. Flywheels have a significant moment of inertia, and thus can resist changes in rotational speed. In this case it is used to maintain constant angular velocity on the crankshaft. It stores energy when torque is exerted on it by the firing engine and it releases energy when the engine does not produce any torque.

Clutch: The clutch is basically two plates pushed together in order to transfer torque to the remaining driveline. When a gear shift is to be made the plates are separated and the torque transfer to the gearbox is terminated. In this thesis the clutch is assumed to be closed at all times and can then be seen as a point mass in the driveline.

Gearbox: The gearbox is a system of linked cogwheels designed to transform the rotational speed and torque in such manner that it matches the specific driving conditions at a certain time.

Propeller shaft: After the gearbox comes the propeller shaft which basically is a long axle that transfer the power from the gearbox to the front or rear of the car. The gear box and the wheel axels are though rarely vertically aligned. This is usually solved by the use of so called universal joints which are capable of transferring rotating motion between two unaligned shafts. Figure 2.6 illustrates the principals of the propeller shaft with the use of the universal joints.

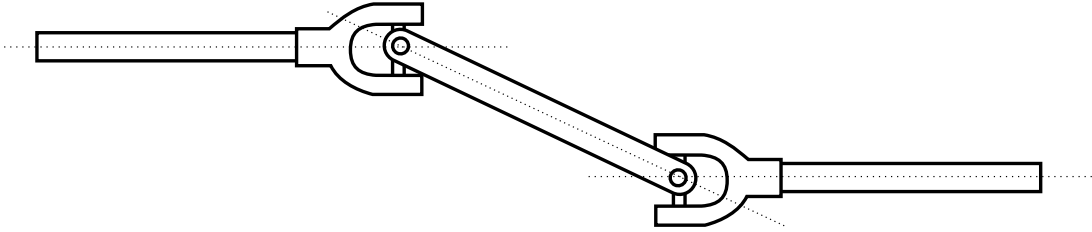


Figure 2.5. Propeller shaft with universal joints.

Differential: The differential is a cog wheel system with the ability of transmitting torque and rotation through three shafts. In this case the three shafts correspond to the propeller shaft as input and the wheel shafts as outputs. It has the ability to allow different speeds on all three shafts, so that the right and rear wheels do not have to have the same angular velocity. A similar device is used in a four wheel driven car to divide the torque between the front and rear wheels.

Wheel shafts: Finally the rotational speed and torque are transferred to the wheel shafts and out to the wheels that then act on the road.

2.3 Tire Pressure Indicator (TPI)

Tire Pressure Indicator (TPI) is a product developed by NIRA Dynamics AB which is a sensor fusion based indirect tire pressure monitoring system. TPI uses already available sensors in the car to create a virtual tire pressure sensor. The signals from a series of sensors for example wheel speed sensors, accelerometers temperature and various engine and power train related signals are sent to a sensor integration unit which merges the information into a virtual pressure sensor. If this sensor indicates a pressure drop in the tires the information are sent to the driver trough the Human-Machine Interface (HMI) and the deflation can be corrected.

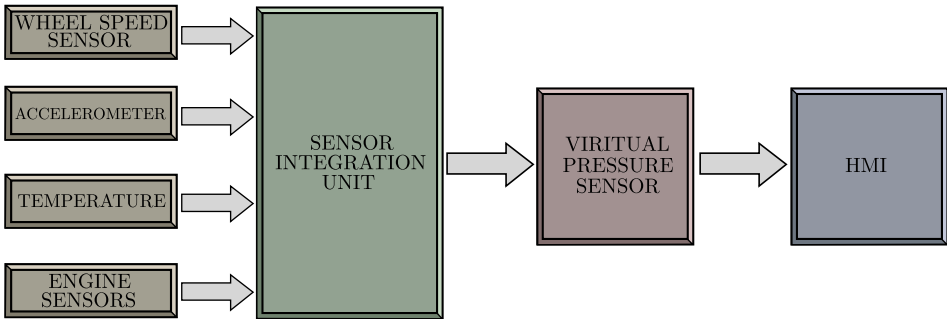
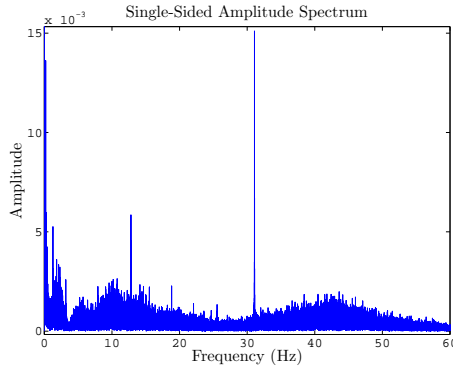


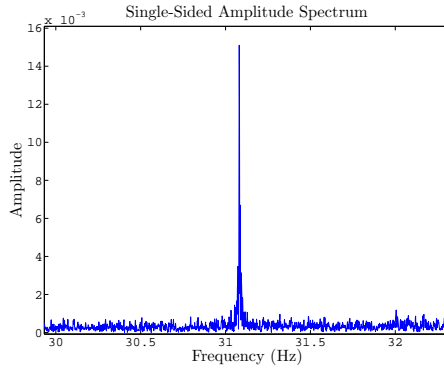
Figure 2.6. Flowchart over the TPI system.

2.4 Desired output

The engine and driveline disturbances that act on the wheel speed often have a characteristic behavior. The characteristics of these disturbances are easiest described in the frequency domain. Figure 2.7 illustrates the spectrum of the wheel speed from a car driving with an engine speed 930 Rounds Per Minute (RPM).



(a) Spectrum of the wheel speed for a car driving with an engine speed of 930 RPM.



(b) Spectrum of the wheel speed for a car driving with an engine speed of 930 RPM, zoomed version.

Figure 2.7. Zoomed and unzoomed version of the wheel speed spectrum for a passenger car, showing a typical narrow banded engine related disturbance.

The engine and driveline related disturbances are shown as narrow banded peaks, usually located at the main engine frequency. The main engine frequency, f_{main} for a four stroke engine is defined in equation (2.1), where N is the number of cylinders and RPM is the engine speed in rounds per minute. There is also sub engine frequencies excited by the engine, these frequencies are not as large as the main engine frequency and the location of these can be found using equation (2.1). In this case N does not represent the number of cylinders but the numbers $N = (1, 2, 3 \dots)$.

$$f_{main} = \frac{RPM \cdot N}{60 \cdot 2} \quad (2.1)$$

As Figure 2.7 shows in this case this results in a peak at 31 Hz. The amplitude and the bandwidth of the disturbance are related to several factors. Engine speed, gear, the dynamics of the system and the engine torque are some of these factors.

2.5 Cylinder shutdown

In the strive of better fuel economy many newer cars have a so called cylinder shutdown ability. The principle is simple, when for example an eight cylinder car do not need all of its cylinders some of them are turned off. This is done by mechanically changing the cam shaft and ignition so that a number of cylinders does not ignite or pump in fuel. The driver does not experience anything different except maybe the engine sound changing. With regard to the previous section a significant change is however done to the main engine frequency. When it comes to detecting and suppressing engine related disturbances on the wheel speed it is therefore crucial to know the number of cylinders that are currently at work, see Example (2.1).

Example 2.1

An eight cylindered car drives with an engine speed of 1200 RPM, Equation (2.1) gives the following main engine frequency:

$$f_{main} = \frac{RPM \cdot N}{60 \cdot 2} = \frac{1200 \cdot 8}{60 \cdot 2} = 80 Hz$$

Four of the eight cylinders are suddenly shutdown in order to save fuel by reducing the number of active cylinders to four. The new main engine frequency would then be:

$$f_{main} = \frac{RPM \cdot N}{60 \cdot 2} = \frac{1200 \cdot 4}{60 \cdot 2} = 40 Hz$$

Equation (2.1) is still valid during cylinder shutdown as long as the number of working cylinders are known.

2.6 Summary and concluding remarks

The most common parts of an ordinary powertrain have been presented and will be modeled in Chapter 3 and 4. The typical behavior of the engine and driveline related disturbances are presented and an expression for the different frequencies that the engine generates is presented. In particular this expression will be useful in Chapter 6, where the effects of the drivelines natural frequencies are discussed.

Chapter 3

The internal combustion engine

3.1 Introduction

In this chapter a mathematical model for describing the output torque from ICEs will be explained. This in order to scrutinise the torque fluctuations causing the wheel speed disturbances. The model will describe four stroke engines, both Spark Ignited (SI) engines and diesel engines. The used model is derived for a SI engine, see [10]. How to parameterise the model in order to describe a diesel engine is however also described in this chapter. The pressure model presented in this chapter will be validated in Chapter 5.

3.2 Four-stroke

The pressure in a four stroke engine cylinder repeat itself in a cycle. One cycle is a 720 degree rotation of the crankshaft and consists of four strokes. When the cycle starts the piston is in its top position, the Top Dead Center (TDC). In this state the crank angle is considered to be zero. An illustration of the four strokes can be seen in Figure 3.1 and a short description of the stokes is provided.

- 1. Intake phase** The inlet valve is opened and the cylinder is moving downwards to the Bottom Dead Center (BDC). An air-fuel mixture is then sucked in to the cylinder.
- 2. Compression phase** The inlet valve closes and the piston moves upward and increasing the pressure in the cylinder. An ignition starts the combustion approximately 20 degrees before TDC.
- 3. Expansion phase** Due to the combustion the piston moves downward (from TDC to BDC) and the combustion finish about 40 degrees after TDC.

4. **Exhaust phase** The outlet valve opens and the burned gases are pushed out of the cylinder when the cylinder moves upward.

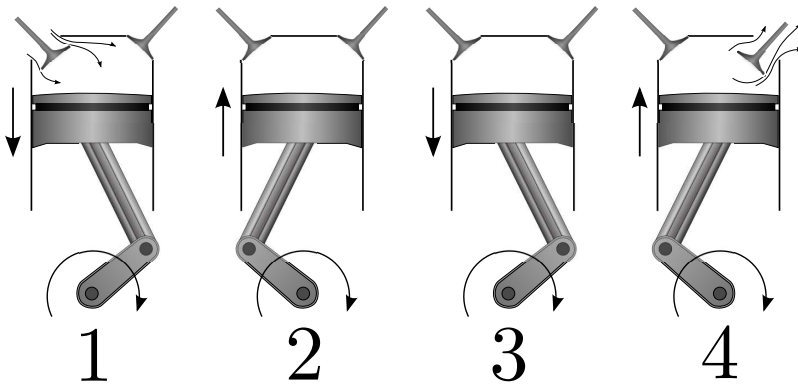


Figure 3.1. The four strokes of a four-stroke engine.

3.3 Cylinder pressure model

In this section a mathematical model describing the pressure in the cylinders of a SI engine is described. The model is mainly a function of the crankshaft angle but also needs knowledge of other parameters e.g. intake manifold pressure and air to fuel ratio λ . To give an illustration of what the model should capture, a typical cylinder pressure, measured from a four cylinders, four stroke, GM Family II engine is shown in Figure 3.2.

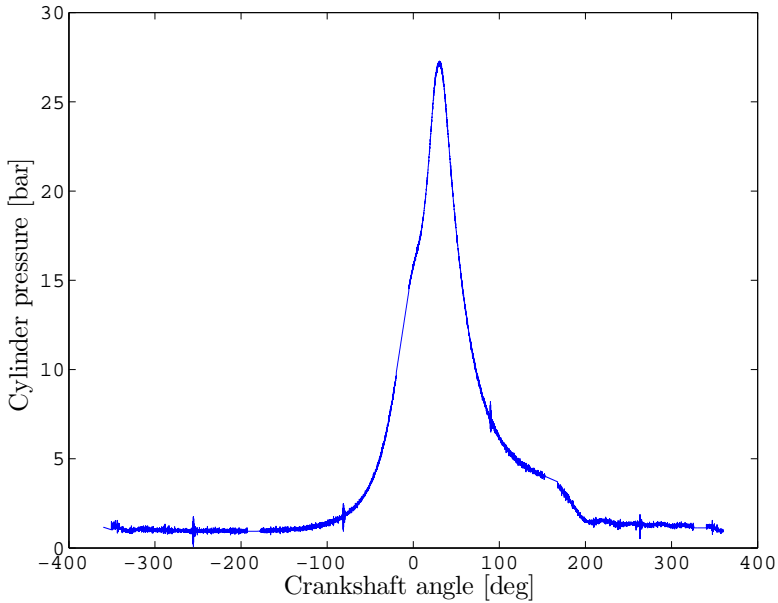


Figure 3.2. Typical cylinder pressure for a SI engine rotating 720 degrees.

The model divides the complete 720 degrees, four stroke cycle into five intervals in which mathematical equations for the pressure is obtained. The intervals are briefly described below and in Figure 3.3 the intervals are presented in a graph.

1. From the Intake Valve Opening (IVO) until Intake Valve Closing (IVC) (the intake phase) the pressure can be approximated by the intake manifold pressure, p_{im} .
2. From IVC to the End of Combustion (EOC) gas is compressed and the compression pressure and temperature are modeled as a polytrophic process. A polytrophic process follows the relation: $pV^n = Constant$ where p is the pressure and V is the volume and n is the polytrophic index. This can take the value of any given real number.
3. At Start of Combustion (SOC) until EOC the pressure is modeled as an interpolation between the compression and expansion pressure.
4. During the expansion phase from EOC to the exhaust valve opens Exhaust Valve Opening (EVO) pressure can also be described as a polytrophic process.
5. Between EVO and exhaust valve closing Exhaust Valve Closing (EVC) which usually occurs about the same time as IVO the pressure can be approximated with the exhaust manifold pressure.

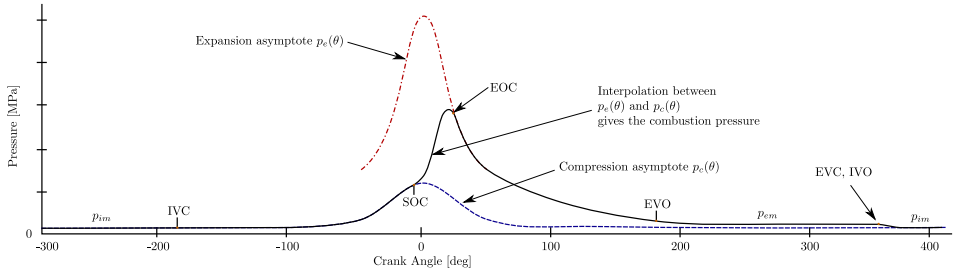


Figure 3.3. Graph showing how the pressure is modeled as one four stroke cycle of a SI engine.

3.3.1 Compression part

When the intake valve closes the compression of the gas begins. The pressure during the compression can be modeled as a polytropic process. This is done under the assumption that the process inside the cylinder can be considered reversible¹ and isentropic². In practice this never happens but it is a well known fact that this particular process can be modeled like this with accurate results, [10].

$$p_c(\theta) = p_{ivc} \left(\frac{V_{ivc}}{V(\theta)} \right)^{k_c} \quad (3.1)$$

$$T_c(\theta) = T_{ivc} \left(\frac{V_{ivc}}{V(\theta)} \right)^{k_c - 1} \quad (3.2)$$

Equation (3.1) and (3.2) describes the pressure and temperature in the time interval from the IVC to when the ignition occurs. Where p and T is the pressure and temperature in the cylinder and the indexes c and ivc refer to the compression part of the cycle and the intake valve closing. The polytropic exponent k_c is a tuning parameter and an expression of the cylinder volume as a function of the crank angle, $V(\theta)$ is derived in Appendix B. The temperature model is needed because it effects the reference pressure in the expansion part of the cycle.

3.3.2 Determination of initial pressure and temperature

In [10] a description of the reference pressure, p_c and temperature T_c is given. The result is simplified models originating from more complex and accurate ones. To maintain simplicity the simplified versions are used in this thesis. The reference pressure is set to the intake manifold pressure at IVC.

$$p_{ivc} = p_{im}(\theta_{ivc}) \quad (3.3)$$

Due to production tolerances the crank angle for intake valve closing is not exactly known and is used as a tuning parameter.

¹A process that can be reversed and causes no change in either the system or its surroundings.

²The entropy of the system remains constant.

During the intake phase the air fuel gas is mixed with the residual gases with temperatures T_{af} and T_r respectively. By assuming that the specific heat for the two gases are equal, the following expression is obtained.

$$T_{ivc} = T_{af}(1 - x_r) + x_r T_r \quad (3.4)$$

Where the residual gas fraction, x_r is defined as the mass of the residual gas divided by the total mass of the gases.

$$x_r = \frac{m_r}{m_a + m_f + m_r} \quad (3.5)$$

Where m stands for mass and the indexes a , f and r are referring to the air, fuel and residual gases in the cylinder. The air-fuel temperature can be approximated by the intake manifold temperature, T_{im} . By assuming that the residual gases experience no loss to the environment, the residual gas temperature, T_r is set equal to the gas temperature at the expansion cycle end, $T_e(EVO)$.

3.3.3 Expansion part

The expansion process is also modeled as polytropic, with the polytropic exponent k_e .

$$p_e(\theta) = p_3 \left(\frac{V_3}{V(\theta)} \right)^{k_e} \quad (3.6)$$

$$T_e(\theta) = T_3 \left(\frac{V_3}{V(\theta)} \right)^{k_e - 1} \quad (3.7)$$

The determination of V_3 , p_3 and T_3 , that refer to state three in the ideal Otto cycle, [11], see Figure 3.4, will be discussed below. State two in the ideal Otto cycle refer to the start of the combustion and state three to the end of combustion. The temperature in state three, T_3 is given by the temperature at state two plus the temperature increase due to combustion, ΔT_{comb} .

$$T_3 = T_2 + \Delta T_{comb} \quad (3.8)$$

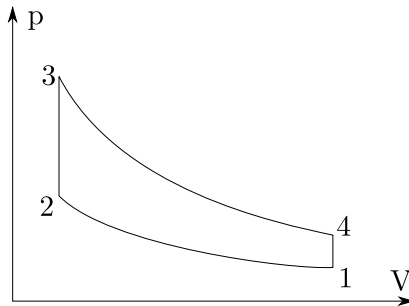


Figure 3.4. Sketch of the ideal Otto cycle that defines the states 2 and 3, referring to the start and end of combustion respectively.

In this approach, the air-to-fuel ratio and the ignition timing, both have an impact on the results. The temperature increase, ΔT_{comb} is given by:

$$\Delta T_{comb} = \frac{m_f q_{HV} \eta_f(\lambda)}{c_v m_{tot}} = \frac{(1 - x_r) q_{HV} \eta_f(\lambda)}{(\lambda(A/F)_s + 1) c_v} \quad (3.9)$$

where m_f is the injected fuels mass, q_{HV} is the fuels heating value, m_{tot} is the total mass of the air, fuel and residual gases, c_v is the specific heat at constant volume, λ is the air-fuel equivalence ratio and $(A/F)_s$ is the stoichiometric air-fuel ratio. For more information of these parameters see [11]. The fuel conversion efficiency $\eta_f(\lambda)$ is given by:

$$\eta_f(\lambda) = 0,95 \min(1; 1, 2\lambda - 0, 2) \quad (3.10)$$

Finally the pressure after the combustion is determined by using the ideal gas law, $pV = nRT$ and realising that the volumes in state two and three in the ideal Otto cycle are the same:

$$p_3 = p_2 \frac{T_3}{T_2} \quad (3.11)$$

where p_2 and T_2 are determined by equations (3.1) and (3.2), meaning:

$$p_2(\theta) = p_{ivc} \left(\frac{V_{ivc}}{V_2} \right)^{k_c} \quad (3.12)$$

$$T_2(\theta) = T_{ivc} \left(\frac{V_{ivc}}{V_2} \right)^{k_c - 1} \quad (3.13)$$

where the phasing of the volume at state two and three are obtained by knowledge of the combustion phase, which requires knowledge of the flame characteristics. Reference [10] takes into account the combustion phasing and [16] describes the flame characteristics, both explained in the next subsection.

3.3.4 Flame characteristics and combustion phasing

The combustion starts with an ignition and ends when the fuel is burned out. This course of event is called flame development and its characteristics and the mass fraction burn rate can be seen in Figure 3.5. A description of the terminology in the figure is explained below.

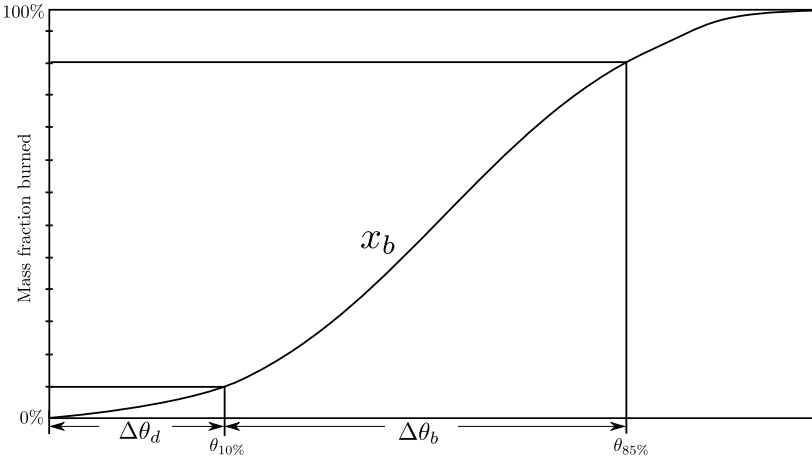


Figure 3.5. The burn profile with definition of the burning angles.

x_b : The burn profile describes how many percent of the fuel has been burnt. This is often described by the Wiebe function, see [11]:

$$x_b(\theta) = 1 - e^{-a \left(\frac{\theta - \theta_{SOC}}{\Delta\theta} \right)^{m+1}} \quad (3.14)$$

Where a and m are calculated as:

$$a = -\ln(1 - 0,1) \left(\frac{\Delta\theta}{\Delta\theta_d} \right)^{m+1} \quad (3.15)$$

$$m = \frac{\ln \left(\frac{\ln(1-0,1)}{\ln(1-0,85)} \right)}{\ln(\Delta\theta_d) - \ln(\Delta\theta_d + \Delta\theta_b)} - 1 \quad (3.16)$$

$\Delta\theta_d$: Flame development angle is the crank angle interval during which flame kernel develops after spark ignition, usually 10% of the mass-fraction burned.

$\Delta\theta_b$: Rapid burn angle is the crank interval when the most of the fuel is burned, usually 10-85% of the mass-fraction burned.

$\Delta\theta$: Combustion duration is the interval of the crank angle when the combustion takes place. An approximation of $\Delta\theta$ is given as: $\Delta\theta = 2\Delta\theta_d + \Delta\theta_b$

The burn angles vary depending on e.g. engine speed, here however they are set constant and are used as tuning parameters.

3.3.5 Method to account for combustion phasing

The ignition timing and the combustion phasing influence the final pressure. Here the combustion phase is adjusted to the burn profile. An expression for the combustion position θ_c is described and motivated in [10].

$$\theta_c = mfb_{50} - MFB_{50,OPT} \quad (3.17)$$

$$mfb_{50} = \Delta\theta_d + \Delta\theta_b/2 \quad (3.18)$$

$$MFB_{50,OPT} = 8^\circ ATDC \quad (3.19)$$

where $MFB_{50,OPT}$ is the optimal point for 50% mass-fraction burned and mfb_{50} is the actual angle for 50% mass-fraction burned. The volumes from state two and three in the Otto cycle are then defined as: $V_2 = V_3 = V(\theta_c)$.

3.3.6 Combustion part

Finally the combustion part is produced by interpolation between the two pressure asymptotes p_c and p_e , c.f. Figure 3.3. The interpolation function is the Wiebe function given in Equation (3.14).

$$PR(\theta) = x_b \quad (3.20)$$

The following expression is then given for the combustion pressure:

$$p(\theta) = (1 - PR(\theta)) \cdot p_c(\theta) + PR(\theta) \cdot p_e(\theta) \quad (3.21)$$

This was the final step in the cylinder pressure model for a four stroke SI engine. In the next subsection a way to parametrise the model to make it resemble a diesel engine is presented. The model will be validated in Chapter 5.

3.3.7 Diesel engine parameterisation

The model presented earlier was derived for a SI engine, it can however also describe diesel engines despite the fundamental difference in the pressure volume relations, this is done with good results in [5]. The differences in the pressure volume relations are illustrated in Figure 3.6.

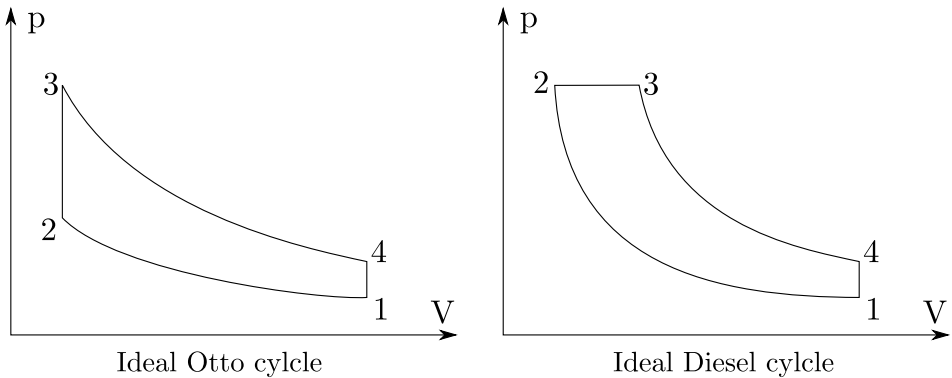


Figure 3.6. The ideal otto and diesel cycle.

When the model should describe a diesel engine it is parameterised in certain way. To do this some critical differences between a petrol engine and a diesel engine should be taken in consideration. Primarily the geometry of the engines differs in such way that the compression ratio, see Equation (3.22), for a petrol engine is in the range from 8 to 12 whilst for the diesel engine it is in the range 12 to 24, [11].

$$\epsilon = \frac{V_{max}}{V_{min}} \quad (3.22)$$

Where ϵ is the compression ratio and V_{min} , V_{max} are the minimum and maximum volume of the cylinder. Due to the fact that the fuel of the diesel engine self ignites the fuel at a high enough pressure, the Start of Combustion (SOC) is often located later (usually around TDC) compared to a petrol engine; the SOC occur approximately at $35^\circ - 0^\circ$ before TDC, [11]. Furthermore, the normalised air to fuel ratio λ^3 is usually 1 for a petrol engine, and above 1.3 and often at values close to 2 for a diesel engine. How well the model can describe a diesel engine will be discussed in Section 5.

3.4 Cylinder pressure torque

When the cylinder gas pressure, P_g is known the generated gas pressure torque T_g , usually referred to as indicated torque can be calculated. An expression for T_g is described in [20]. Figure 3.7 illustrates the acting forces on the crank-shaft due to p_g .

³ λ is defined as $\lambda = \frac{(m_a/m_f)}{(m_{a,s}/m_{f,s})}$ where m_a and m_f are the mass of the cylinders air and fuel, $m_{a,s}$ and $m_{f,s}$ are the mass of air and fuel it takes for a complete reaction between the air and fuel, i.e. all air and fuel are burnt.

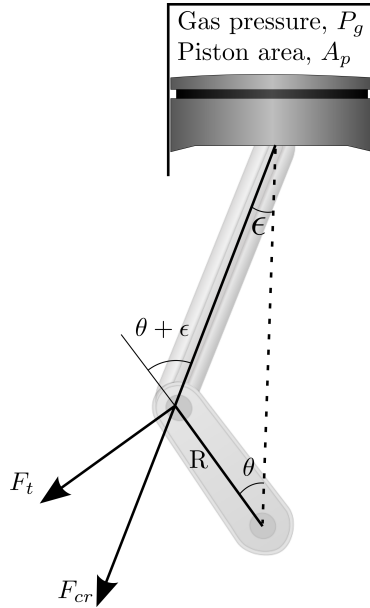


Figure 3.7. Illustration of the slider-crank mechanism.

The force acting on the crank, F_{cr} is described in (3.23) and the force perpendicular to the crank F_t is given in (3.24). To obtain the torque the force is then multiplied with the crank radius (3.25), [20].

$$F_{cr} = \frac{P_g A_p}{\cos \epsilon} \quad (3.23)$$

$$F_t = F_{cr} \sin \epsilon + \theta \quad (3.24)$$

$$T_g(\theta) = F_t R \quad (3.25)$$

Where F_{cr} , P_g , A_p , F_t , R , ϵ and θ are specified in Figure 3.7

3.5 Summary and concluding remarks

A model that describes the pressure curve in an engine cylinder has been presented. It was derived for spark ignited engines but can be parameterised for usage on diesel engines as well. Further more the cylinder pressure is used to calculate the generated torque on the crankshaft. This torque is used as an input to the driveline model presented in the next chapter.

Chapter 4

Driveline

4.1 Introduction

In this chapter a driveline model capable of describing the wheel speed oscillations as a function of the applied torque on the crankshaft will be derived. The model is based on El-Adl Mohammed Aly Rabeihs Ph.D. thesis in which he derives a discretised and lumped mass model in order to investigate the torsional vibrations and rotating speed fluctuations in a driveline [20]. The model is then further developed, converting it from a two wheel driven car to a four wheel driven. Functionality regarding gear shifts and wheel slip is also added.

4.2 Original two wheel drive model

The model described in [20] basically consists of a series of masses and dampers connected to each other with stiff springs. In Figure 4.1 the mathematical model of the driveline is illustrated, showing how the different parts in the driveline have been simplified into a equivalent system of masses, springs and dampers.

$K_2 =$

$$\begin{pmatrix} 0 & 0 & 0 & 0 & 0 & 0 & 0 & 0 \\ 0 & & & & & & & 0 \\ 0 & & & & & & & 0 \\ 0 & & & & & & & 0 \\ 0 & & & & & & & 0 \\ 0 & & & & & & & 0 \\ -k_7 & & & & & & & 0 \\ k_7 + k_8 & -k_8 & & & & & & 0 \\ -k_8 & k_8 + k_9 & -k_9 & & & & & 0 \\ & -k_9 & k_9 + k_{10} & -k_{10} & & & & 0 \\ & & -k_{10} & k_{10} + k_{11} & -k_{11} & & & 0 \\ & & & -k_{11} & k_{11} + k_{12} + k_{13} & -k_{13} & -k_{12} & 0 \\ & & & & -k_{13} & k_{13} + k_{15} & 0 & 0 \\ 0 & 0 & 0 & 0 & -k_{12} & 0 & k_{12} + k_{14} & 0 \end{pmatrix}$$

 $C =$

$$\begin{pmatrix} c_1 & -c_1 & 0 & 0 & 0 & 0 & 0 & 0 & 0 \\ -c_1 & c_1 + c_2 & & & & & & & 0 \\ 0 & & c_3 & & & & & & 0 \\ 0 & & & \ddots & & & & & 0 \\ 0 & & & & c_6 & & & & 0 \\ 0 & & & & & c_6 + c_7 & & & 0 \\ 0 & & & & & & c_8 & & 0 \\ 0 & & & & & & & \ddots & 0 \\ 0 & 0 & 0 & 0 & 0 & 0 & 0 & 0 & c_{14} \end{pmatrix}$$

 $M =$

$$\begin{pmatrix} J_1 & 0 & 0 \\ 0 & \ddots & 0 \\ 0 & 0 & J_{14} \end{pmatrix}$$

In Table 4.1 parameter values are given for mass moment of inertia, damping and stiffness for a typical passenger car [20].

Equivalent stiffness coefficient (Nm/rad)		Equivalent moment of inertia ($Kg \cdot m^2$)		Equivalent system damping coefficient ($Nm \cdot s/rad$)	
Parameter	Value	Parameter	Value	Parameter	Value
k_1	$0,2 \cdot 10^6$	J_1	0,3	c_1	3
k_2	$1 \cdot 10^6$	J_2	0,03	c_2	2
k_3	$1 \cdot 10^6$	J_3	0,03	c_3	2
k_4	$1 \cdot 10^6$	J_4	0,03	c_4	2
k_5	$1 \cdot 10^6$	J_5	0,03	c_5	2
k_6	$0,05 \cdot 10^6$	J_6	1,0	c_6	4,42
k_7	$2 \cdot 10^6$	J_7	0,05	c_7	1
k_8	$1 \cdot 10^6$	J_8	0,03	c_8	1
k_9	$0,1 \cdot 10^6$	J_9	0,05	c_9	1
k_{10}	$0,1 \cdot 10^6$	J_{10}	0,02	c_{10}	1,8
k_{11}	$0,2 \cdot 10^6$	J_{11}	0,02	c_{11}	1,8
k_{12}	$0,5 \cdot 10^4$	J_{12}	0,3	c_{12}	2
k_{13}	$0,5 \cdot 10^4$	J_{13}	2	c_{13}	10
k_{14}	$0,2 \cdot 10^4$	J_{14}	2	c_{14}	10
k_{15}	$0,2 \cdot 10^4$				

Table 4.1. Typical values for parameters of the vehicle driveline model.

4.3 Four wheel drive model

To widen the range of vehicles that are possible to simulate the model is extended to a four wheel drive model. This is done by simply adding an additional set of propeller shaft and final drive system. Since the wheels are connected to a fixed non moving point and just oscillates around zero there is no need for a model of a differential allowing the wheels to spin at different speeds. It is however crucial that the torque acting on the front and rear axis of the model is adjustable in order to obtain the correct amplitude of the disturbances. This will be discussed later in this chapter and Figure 4.2 illustrates the four wheel drive model.

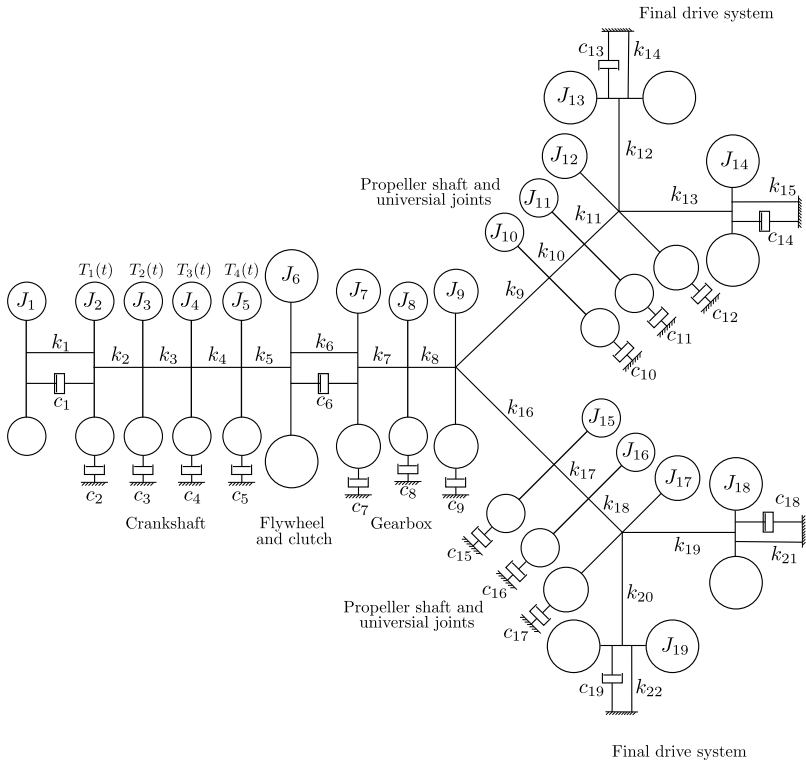


Figure 4.2. Illustration of the four wheel drive model showing the different parts of the driveline as a system of masses, springs and dampers.

The moment of inertia, damping and stiffness matrices for the four wheel drive model are presented below.

$$K = \begin{pmatrix} K_1 & K_2 \end{pmatrix}$$

$K_2 =$

$$\begin{pmatrix} 0 & 0 & 0 & 0 & 0 & 0 & 0 & 0 & 0 \\ 0 & & & & & & & & 0 \\ 0 & & & & & & & & 0 \\ 0 & & & & & & & & 0 \\ 0 & & & & & & & & 0 \\ 0 & & & & & & & & 0 \\ 0 & & & & & & & & 0 \\ 0 & & & & & & & & 0 \\ 0 & & & & -k_{16} & & & & 0 \\ 0 & & & & & & & & 0 \\ -k_{11} & & & & & & & & 0 \\ k_{11}+k_{12}+k_{13} & -k_{13} & -k_{12} & & & & & & 0 \\ -k_{13} & k_{13}+k_{15} & & & & & & & 0 \\ -k_{12} & 0 & k_{12}+k_{14} & & & & & & 0 \\ 0 & & & k_{16}+k_{17} & -k_{17} & & & & 0 \\ 0 & & & -k_{17} & k_{17}+k_{18} & -k_{18} & & & 0 \\ 0 & & & & -k_{18} & k_{18}+k_{19}+k_{20} & -k_{19} & -k_{20} & 0 \\ 0 & & & & & -k_{19} & k_{19}+k_{21} & 0 & 0 \\ 0 & 0 & 0 & 0 & 0 & -k_{20} & 0 & k_{20}+k_{22} & 0 \end{pmatrix}$$

$C =$

$$\begin{pmatrix} c_1 & -c_1 & 0 & 0 & 0 & 0 & 0 & 0 & 0 \\ -c_1 & c_1 + c_2 & & & & & & & 0 \\ 0 & & c_3 & & & & & & 0 \\ 0 & & & \ddots & & & & & 0 \\ 0 & & & & c_6 & & & & 0 \\ 0 & & & & & c_6 + c_7 & & & 0 \\ 0 & & & & & & c_8 & & 0 \\ 0 & & & & & & & \ddots & 0 \\ 0 & 0 & 0 & 0 & 0 & 0 & 0 & 0 & c_{19} \end{pmatrix}$$

$M =$

$$\begin{pmatrix} J_1 & 0 & 0 \\ 0 & \ddots & 0 \\ 0 & 0 & J_{19} \end{pmatrix}$$

4.4 Front and rear system parameters

In order to investigate the characteristics of the disturbances on the front and the rear wheels in a four wheel driven car a convenient way of choosing the parameters for the front and rear system are derived. The method yields the following plausible assumptions:

- The main difference between the front and the rear systems lies in the propeller shafts and not in the final drive system.
- All the rotating parts of the propeller shaft can be seen as cylinders rotating around its own axis.
- The main difference between the front and rear propeller shaft is that the front propeller shaft is shorter.

The mass moment of inertia and stiffness of a cylinder are presented in equation (4.2)-(4.3).

$$J = \frac{1}{32}\pi\rho lD^4 \quad (4.2)$$

where J is the mass moment of inertia, ρ is the density of the material, l is the length of the cylinder and D is the cylinder diameter. The torsional stiffness of the cylinder, k is given by:

$$k = \frac{J_T}{l}G \quad (4.3)$$

where G is the modulus of rigidity¹, l is the length of the cylinder and J_T is the second moment of area, defined below in equation (4.4), where D is the cylinder diameter.

$$J_T = \frac{1}{2}\pi D^4 \quad (4.4)$$

As equations (4.2)-(4.3) show the mass moment of inertia is proportional to the length of the cylinder and the torsional stiffness is inversly proportional to the length of the cylinder. This means that the relationship between the length of the rear propeller shaft, l_r and the front propeller shaft length, l_f can be expressed as: $l_f = l_r \cdot x$, where $x \in]0, 1]$. The relationship between the front and rear stiffness and inertia, k_f , k_r , J_f and J_r can therefore be explained by (4.5)-(4.6).

$$k_f = \frac{k_r}{x}, \quad (4.5)$$

$$J_f = J_r x. \quad (4.6)$$

Since the parameters presented in Table 4.1 are refering to a rear wheel driven car the additional parameters due to the four wheel expansion can be expressed by the previously mentioned method; the results are presented in Table 4.2.

¹The modulus of rigidity is a material specific constant.

Equivalent stiffness coefficient (Nm/rad)		Equivalent moment of inertia ($Kg \cdot m^2$)		Equivalent system damping coefficient ($Nm \cdot s/rad$)	
Parameter	Value	Parameter	Value	Parameter	Value
k_{16}	k_9/x	J_{15}	$J_{10}x$	c_{15}	c_{10}
k_{17}	k_{10}/x	J_{16}	$J_{11}x$	c_{16}	c_{11}
k_{18}	k_{11}/x	J_{17}	J_{12}	c_{17}	c_{12}
k_{19}	k_{12}	J_{18}	J_{13}	c_{18}	c_{13}
k_{20}	k_{13}	J_{19}	J_{14}	c_{19}	c_{14}
k_{21}	k_{14}				
k_{22}	k_{15}				

Table 4.2. Values for the additional front drive system parameters using the fact that the front propeller shaft is considerably shorter than the rear propeller shaft.

4.5 Gear dependency

The original model, [20] does not include different gears in the car. By looking at measurements from the database at NIRA Dynamics AB it can be concluded that the choice of gear heavily affect the amplitude of the wheel speed disturbance. The disturbances increase, as could be expected with higher gears. A higher gear decreases the transferred torque but since it increases the rotational speed the wheel speed disturbance increases. For this reason a possibility to choose gear is implemented in the equivalent gearbox system of the model. This is implemented as a gain that correspond to the gear ratio of the car. An illustration of this can be seen in Figure 4.3.

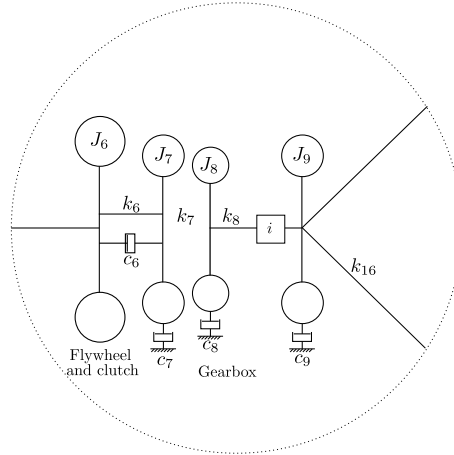


Figure 4.3. Illustration of the implemented gear shift capability of the model, where i is the gear ratio.

4.6 Transferred torque and slip

By experiments with the model it can be seen that when the parameters of the front and rear system is the same the torque transferred to the front and rear wheels are the same. As previously mentioned this is however not the case since the parameters in the front and rear systems are likely to differ from each other. This results in an incorrect torque on the front and rear propeller axes and wheels, which in turn leads to incorrect disturbance amplitudes. In a real car the torque transfer to the wheels are determined by the force needed to maintain the current acceleration and speed of the vehicle, often called tractive force. Since the model does not describe a moving vehicle but rather the wheel speed variations, the torque division between the front and the rear of the system are determined by the dynamics of the system. To avoid this phenomenon a torque that corresponds to one that a theoretical² vehicle speed and acceleration would generate is applied on the wheels. The tractive force F_t can be calculated by the following equation [11]:

$$F_t = m\dot{v} + \frac{1}{2}c_w A_a \rho_a v^2 + mc_r + mg \sin \alpha \quad (4.7)$$

where c_r and c_w are the rolling and air resistance constants, m is the car mass, v is the velocity, A_a is the frontal area of the car, ρ is the air density, g is the gravitational constant and α is the road angle. How this force is divided between the four wheels depends on several factors but one of the primary factors are the wheel slip which will be discussed in the next section.

²The theoretical vehicle speed and acceleration can be calculated by knowing the engine speed and gear.

4.6.1 Slip

The driven wheels on a car do not roll, instead they rotate faster than the corresponding longitudinal velocity. This velocity difference is called longitudinal slip, or simply slip. The slip is described by the slip factor s and is defined as:

$$s = \frac{r_0\omega - v}{r_0\omega} \quad (4.8)$$

where r_0 is the effective wheel radius, ω is the angular velocity of the wheels and v is the absolute vehicle velocity, [11].

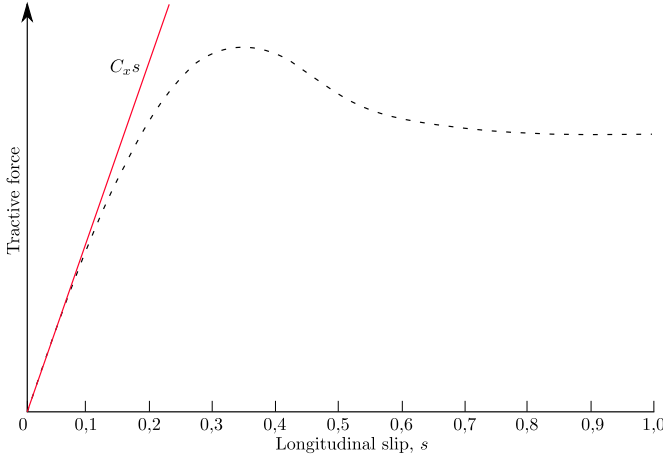


Figure 4.4. Illustration of the tractive force as a function of slip (dashed) and its approximation for low slip values (solid).

How this force is divided on the wheels as a function of slip can be seen as the dashed line in Figure 4.4. It is however often sufficient to assume that the slip is low and can therefore be approximated to be linear as the solid line in Figure 4.4 [14]. For simplicity this assumption is made in this thesis and the equation for the tractive force on one tire as a function of slip is given by equation:

$$F_{w,i} = C_x s \quad (4.9)$$

where C_x is the effective longitudinal stiffness of the tire. The index $i \in \{1, 2, 3, 4\}$ represents one of the four tires. Finally to calculate the torque that is applied on the wheels, T_w the force is multiplied with the effective wheel radius, r_0

$$T_{w,i} = F_{w,i} r_0 \quad (4.10)$$

The result of this is that we obtain a model with a controllable torque distribution on the wheels and the ability to investigate the consequences of slip. The resulting force vector \mathbf{F} in equation (4.1) are presented below, where T_{1-4} are the fluctuating engine torque and $T_{w,1-4}$ is the tractive torque discussed in this section. $\mathbf{T} =$

$$\left(T_1(t) \quad T_2(t) \quad T_3(t) \quad T_4(t) \quad \cdots \quad T_{w,1}(t) \quad T_{w,2}(t) \quad \cdots \quad T_{w,3}(t) \quad T_{w,4}(t) \right)^T$$

4.7 Natural frequencies

When the motored frequencies of a system (here the engine torque, see equation (2.1)) coincides with the natural frequencies³ a resonance phenomena occurs and the disturbances are amplified. It is therefore crucial in order to analyse the system properly to be able to calculate these frequencies. Nickmehr [17] describes a way of calculating the undamped natural frequencies (not including the viscous damping of the system). A comparison is then made to reference [20] that calculates the damped natural frequencies. The result shows that the undamped natural frequencies corresponds well to the damped and for the purpose of simplicity the undamped natural frequency calculations are chosen for this thesis. By excluding the applied force and the damping in equation (4.1) and realising that for an undamped system \mathbf{x} is sinusoidal and can therefore be replaced with $\mathbf{X}e^{i\omega t}$ we get:

$$-\omega^2 \mathbf{M}\mathbf{X}e^{i\omega t} + \mathbf{K}\mathbf{X}e^{i\omega t} = 0 \quad (4.11)$$

and by removing the scalar value $e^{i\omega t}$,

$$-\omega^2 \mathbf{M}\mathbf{X} + \mathbf{K}\mathbf{X} = 0 \quad (4.12)$$

In order to solve equation (4.12) it is converted to the form $\mathbf{A}\mathbf{X} = \lambda\mathbf{X}$ which is the familiar form for Eigen-value problems. To do so, both sides of equation (4.12) are multiplied by the term \mathbf{K}^{-1} from the left as follows:

$$-\omega^2 \mathbf{K}^{-1}\mathbf{M}\mathbf{X} + \mathbf{K}^{-1}\mathbf{K}\mathbf{X} = 0 \quad (4.13)$$

or

$$-\omega^2 \mathbf{K}^{-1}\mathbf{M}\mathbf{X} + \mathbf{I}\mathbf{X} = 0 \quad (4.14)$$

and finally we obtain:

$$\mathbf{K}^{-1}\mathbf{M}\mathbf{X} + 1/\omega^2 \mathbf{X} = 0 \quad (4.15)$$

in this case $\mathbf{A} = \mathbf{K}^{-1}\mathbf{M}$ and $\lambda = 1/\omega^2$. Therefore the natural frequencies of the system are the inverse of the positive square roots of the Eigen-values of matrix \mathbf{A} . When using the model parameters presented in this chapter the two wheel drive and the four wheel drive models result in 14 and 19 natural frequencies respectively. The natural frequencies that are below 400Hz from the two systems are presented below in Table 4.3 and 4.4.

Natural frequency (Hz)					
4,03	9,42	12,59	50,856	109,68	139,04

Table 4.3. Natural frequency (Hz) of the two wheel drive model.

³The natural frequency is the frequency at which a system naturally vibrates once it has been set into motion.

Natural frequency (Hz)								
4,37	8,92	9,42	9,42	15,04	46,34	74,05	111,21	212,84

Table 4.4. Natural frequency (Hz) of the four wheel drive model.

It should be noted that this is based on the parameters obtained from [20] and does not necessarily represent the reality. It is not an easy task to obtain these parameters for an arbitrary vehicle and the parameters do not show any extreme values and can be said to be general enough to at least be seen as a good starting point. These parameters are after all better than no parameters at all.

4.8 Summary and concluding remarks

The two wheel drive model originally presented in [20] has been expanded to a model of the driveline of a four wheel drive vehicle. Features have been added, such as the ability to include slip and selection of gears in the model. This is the final part of the complete powertrain model used in this thesis; in the next chapter the entire powertrain model will be validated.

Chapter 5

Validation

5.1 Measurements

The measurements used to validate the model were conducted in the engine laboratory the Vehicle Systems section at LiU and in a test rig located in the Vehicle laboratory at LiU. The experiments in the engine lab were conducted on a four stroke, GM family SI engine in order to validate the cylinder pressure model explained in Chapter 3. The measurements in the test rig were made on two different four wheel driven cars, one Audi A4 TDI with a diesel engine and one Audi A5 TFSI with a petrol engine. These tests were made in order to validate the entire powertrain model. In this chapter the specific engine speeds that were used in the validating process will not be spelled out at the request of NIRA Dynamics AB.

5.1.1 Setup in the engine lab

In the engine laboratory measurements were made on a free standing four stroke, GM family SI engine. The engine could be set to a specific engine speed and torque and measurements were then done on the cylinder pressure, intake manifold pressure and exhaust pressure. Measurements were made at two different engine speeds in the lower region, RPM1 and RPM2 ($RPM2 = 2 \cdot RPM1$).

5.1.2 Setup in the vehicle lab

The existing sensors in the cars were used during the experiments and the main signal used are the wheel speed for all four wheels sampled at 200 Hz. In the test rig it is possible to drive the car while standing still. To do so the wheels of the cars are removed and electrical motors are mounted on the wheel hubs. By doing this all disturbances related to road irregularities and the tires are eliminated. It is possible to run the electrical motors in two modes, road simulation and fixed wheel speed. In the road simulation mode the electrical motors apply a braking torque corresponding to the torque generated from the road at the current speed.

In the second mode the electrical motors are set to a wheel speed and maintains this regardless of the applied torque from the engine. Figure 5.1 illustrates the test set-up.

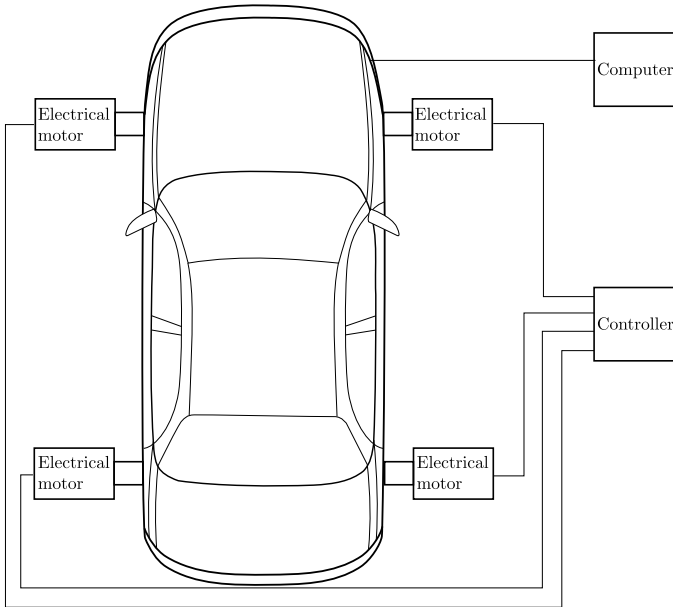


Figure 5.1. Illustration of the test-setup, the controller logs data from the electrical motors and controls these, while the computer takes care of the data collection from the car.

5.1.3 Tests

This section will describe the execution and objective of the conducted tests. If nothing else is stated the cars were driven with a torque distribution between the front and the rear wheels of 50:50.

Test1

Objective: Examine the amplitude and frequency change as a function of engine speed and selected gear.

Methodology: The diesel car, Audi A4 TDI was used and the test rig was set to road simulation. The car was then driven at different engine speeds and at all gears. Table 5.1 specifies at which engine speeds and gears the tests were conducted.

Test No.	Engine speed [RPM]	Gear
1	T1:RPM1, T1:RPM2, T1:RPM3, T1:RPM4, T1:RPM5	1
2	T1:RPM1, T1:RPM2, T1:RPM3, T1:RPM4, T1:RPM5	2
3	T1:RPM1, T1:RPM2, T1:RPM3, T1:RPM4, T1:RPM5	3
4	T1:RPM1, T1:RPM2, T1:RPM3, T1:RPM4, T1:RPM5	4
5	T1:RPM1, T1:RPM2, T1:RPM3, T1:RPM4, T1:RPM5	5
6	T1:RPM1, T1:RPM2, T1:RPM3, T1:RPM4, T1:RPM5	6

Table 5.1. Description of which engine speeds and gears that where used during Test1.

Test2

Objective: Examine the difference in wheel speed disturbances for petrol and diesel cars.

Methodology: The torque on the wheels where set to road simulation. The used car was petrol driven, AUDI A5 TFSI and it was driven for different engine speeds at gear 4. For comparison with a diesel car measurement 3 from Test1 is used. This contains the same engine speed but at gear 3. This is because gear 4 in the car used in this test and gear 3 for the car in Test1 has approximately the same gear ratio. Measurements at gears 2 and 3 where then made for further validation of the diesel engine model. Table 5.2 specifies at which engine speeds and gears the test where conducted.

Test No.	Engine speed [RPM]	Gear
1	T2:RPM1, T2:RPM2, T2:RPM3	4
2	T2:RPM1, T2:RPM2, T2:RPM3	2
3	T2:RPM1, T2:RPM2, T2:RPM3	3

Table 5.2. Description of which engine speeds and gears that where used during Test2.

Test3a/b

Objective: Investigate how large effect potential resonance phenomenon has on the wheel speed disturbance.

Methodology: The natural frequencies of the driveline is estimated in Table 4.4, but is considered unknown, so to investigate if there will occur a resonance peak and how large it will be a sweep over an engine speed interval was made. This where done in both cars and the sweep where conducted by continuously accelerating the car with the gas pedal in the interval T3:RPM1 - T3:RPM2 which corresponds to excitations in the interval 33-100Hz, according to Equation (2.1). The car where driven at gear 4 and the test in which the petrol car was used will be refered to as Test3a and the test with the diesel car will be refered to as Test3b.

Test4

Objective: Examine how the disturbance changes in amplitude for different gears when applying a constant engine torque.

Methodology: The fixed engine speed mode was used in the rig and the Audi A4 TDI was the used car. The car was then driven at different engine speeds and with a fixed engine torque, 50 Nm. At each engine speed every feasible gear in the car was tested. Table 5.3 specifies at which engine speeds and gears the tests where made.

Test No.	Engine speed [RPM]	Gear
1	T5:RPM1	4, 5, 6
2	T5:RPM2	2, 3, 4, 5, 6
3	T5:RPM3	2, 3, 4, 5, 6
4	T5:RPM4	2, 3, 4, 5, 6

Table 5.3. Description of engine speeds and gears that where used during Test4.

5.2 Engine

In this section the cylinder pressure model will be validated, it was validated against the measurements made in the engine laboratory at LiU. The parameters used for the simulations are presented below followed by the simulated cylinder pressure curves compared to the measured ones. The SI engine validation will then be followed by a validation of the diesel engine model.

General simulation parameters

Many parameters were not changed from the two simulations and they are presented in the table below:

Parameter	Symbol	Value
Air-Fuel ratio	λ	1
Crankshaft radius	r	45[mm]
Connecting rod length	l	147[mm]
Piston area	A_p	$52,8 \cdot 10^{-4}[m^2]$
Cylinder clearance volume	V_{cl}	$6,29 \cdot 10^{-5}[m^3]$
Residual gas fraction	x_r	0,1
IVC	θ_{IVC}	180°
Fuel heating value	q_{HV}	$45 \cdot 10^6[J/kg]$

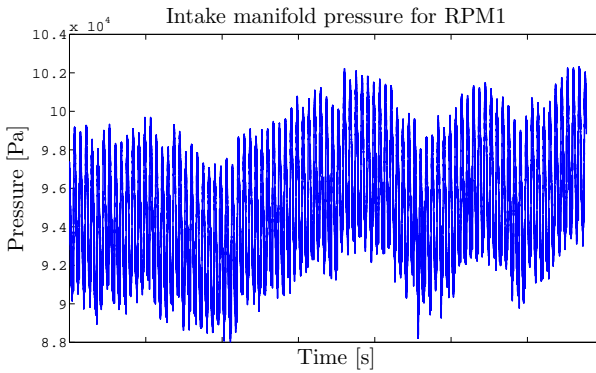
Table 5.4. General parameter values used in both simulations.

Specific simulation parameters for RPM1

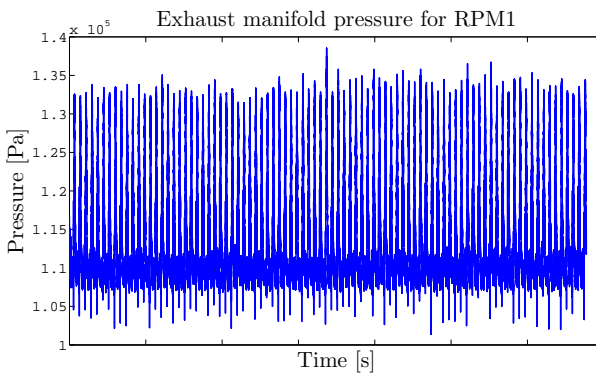
The parameters specific for the RPM1 simulation are presented here. These parameters are difficult to know the exact value of and are seen as tuning parameters.

Parameter	Symbol	Value
SOC	θ_{SOC}	$35^\circ BTDC$
Flame development angle	θ_d	10°
Rapid burn angle	θ_b	20°

Table 5.5. Parameter values used in the RPM1 simulation.



(a) Intake manifold pressure.



(b) Exhaust manifold pressure.

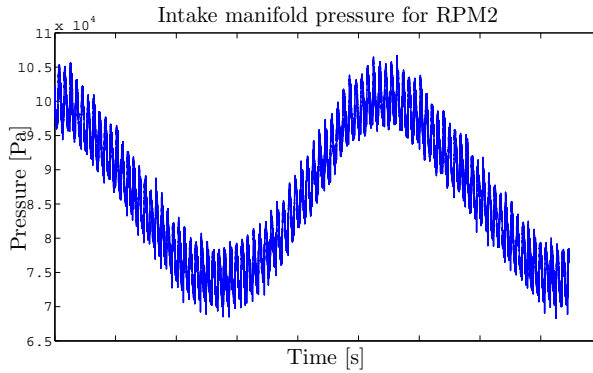
Figure 5.2. The intake and exhaust pressure used for the RPM1 simulation.

Specific simulation parameters for RPM2

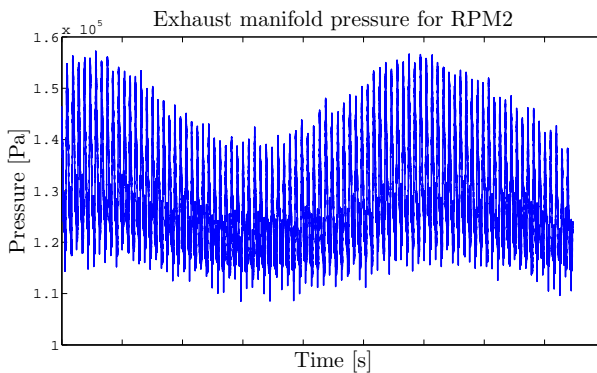
The parameters specific for the RPM2 simulation are presented here. These parameters are difficult to know the exact value of and are seen as tuning parameters.

Parameter	Symbol	Value
SOC	θ_{SOC}	$35^\circ BTDC$
Flame development angle	θ_d	10°
Rapid burn angle	θ_b	18°

Table 5.6. Parameter values used in the RPM2 simulation.



(a) Intake manifold pressure.

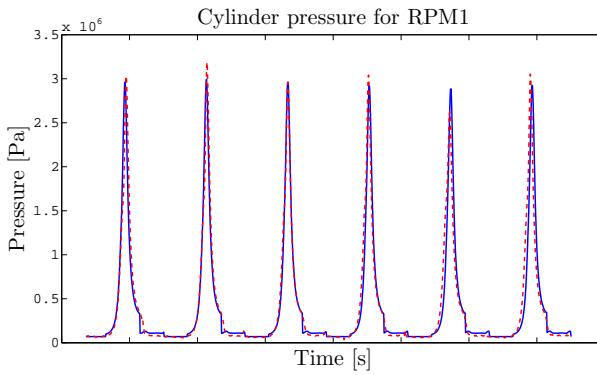


(b) Exhaust manifold pressure.

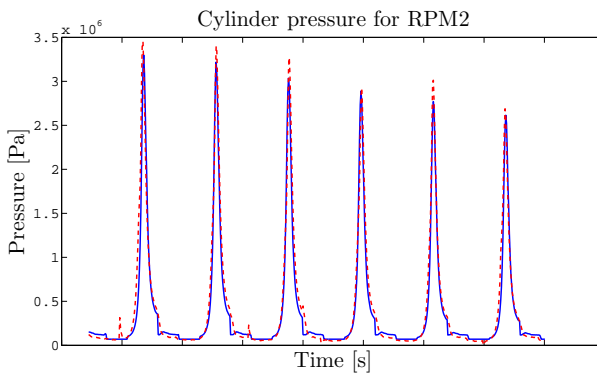
Figure 5.3. The intake and exhaust pressure used for the RPM2 simulation.

Simulation

The engine model was used to simulate the pressure in one cylinder for RPM1 and RPM2 and a comparison between the simulated and measured pressure can be seen in Figures 5.4-5.5.

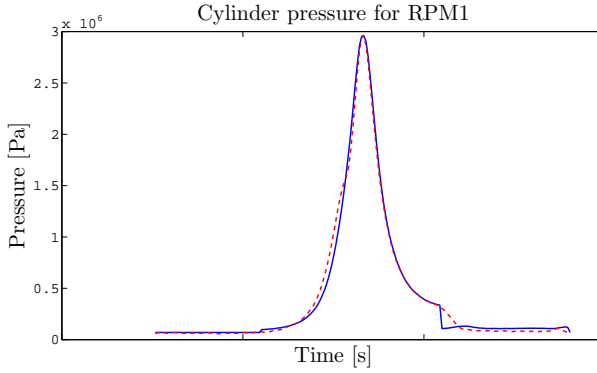


(a) Comparison at RPM1.

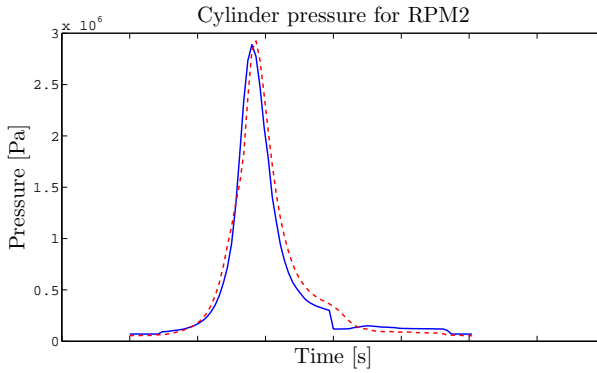


(b) Comparison at RPM2.

Figure 5.4. The cylinder pressure for several engine rotations, measured (Red, dashed) and simulated (Blue, solid).



(a) Comparison at RPM1.



(b) Comparison at RPM2.

Figure 5.5. The cylinder pressure for one pressure peak (720 degrees rotation of crankshaft), measured (Red, dashed) and simulated (Blue, solid).

When the exhaust valve is opened the modeled pressure in the cylinder drastically drops to the pressure in the exhaust manifold. In the real cylinder the pressure drop is not instant, this is illustrated in Figure 5.6.

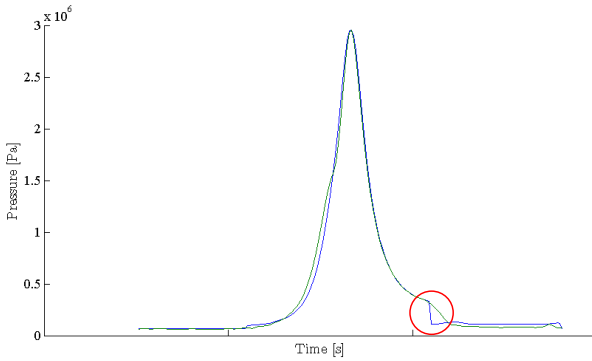


Figure 5.6. Illustration of the pressure differences of the simulations and the measurements when the exhaust valve opens.

This is the largest flaw in the model but does not have as large effect on the produced torque as one could think. When the exhaust valve is opened the piston is in very close to its lower position and the crankshaft is in such angle that it cannot produce very much torque. This and the relatively low pressure in the cylinder at the time make the sudden pressure drop negligible in a torque production point of view. The modeled cylinder pressure however shows good resemblance to the measured pressure.

5.2.1 Diesel engine model

There are no measurement available to validate the ability of the engine model to describe a diesel engine. J. Scarpati et al. in 2007, however used the same model to describe the cylinder pressure in an inline 6-cylinder diesel engine, [5]. In the report a comparison between the model output and measured cylinder pressure is done for three different engine speeds, see Figure 5.7. The figure shows promising result for the simulated and measured cylinder pressure resemblance.

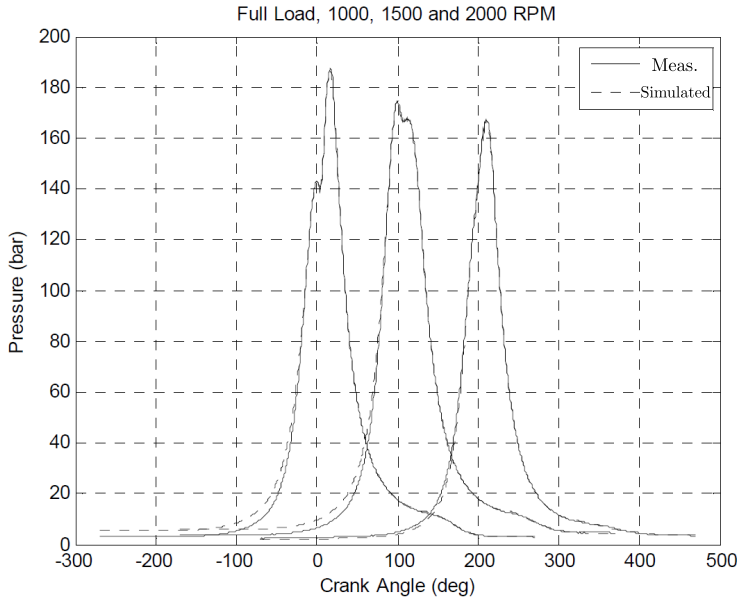


Figure 5.7. Measured and estimated pressure traces. From left to right 1000 RPM, 1500 rpm, 2000 RPM respectively, [5].

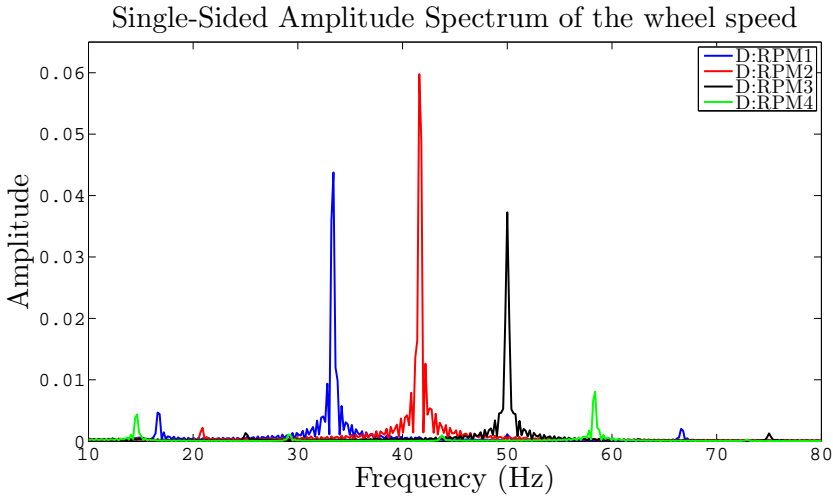
5.3 Driveline

The driveline model was validated against data from Test4, see Section 5.1.3. In the validation the measured results are compared to the simulated results from the entire model including the engine. Twelve different operating points regarding gear and engine speeds are compared. The engine specific parameters in the engine model matches the ones in the real engine and the parameters can be seen in Table 5.7. The parameters in the driveline model are the ones presented in Table 4.1 and 4.2.

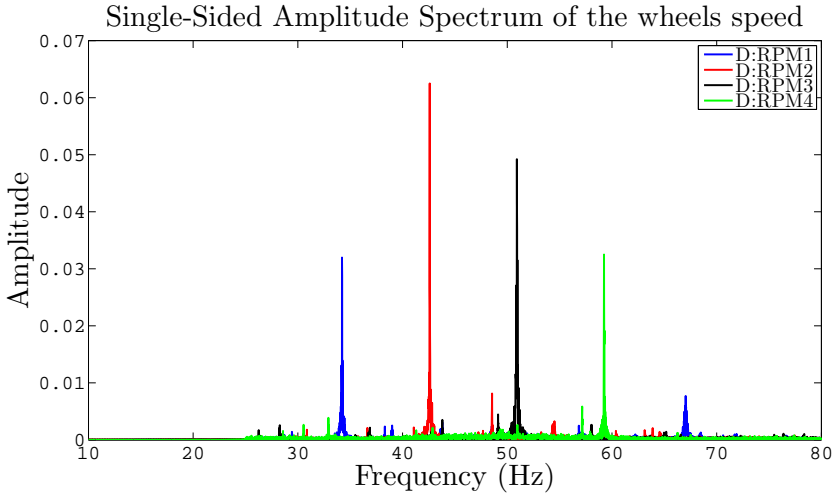
Parameter	Value
Displacement	1968 cm^3
Bore	81 mm
Stroke	95.5 mm
Compression ratio	16,5:1

Table 5.7. Geometrical engine parameters used for the simulation.

Figures 5.8-5.10 show the wheel speed spectrum of the measured and simulated results for a car driving in D:RPM1, D:RPM2, D:RPM3 and D:RPM4 at 4:th, 5:th and 6:th gear.

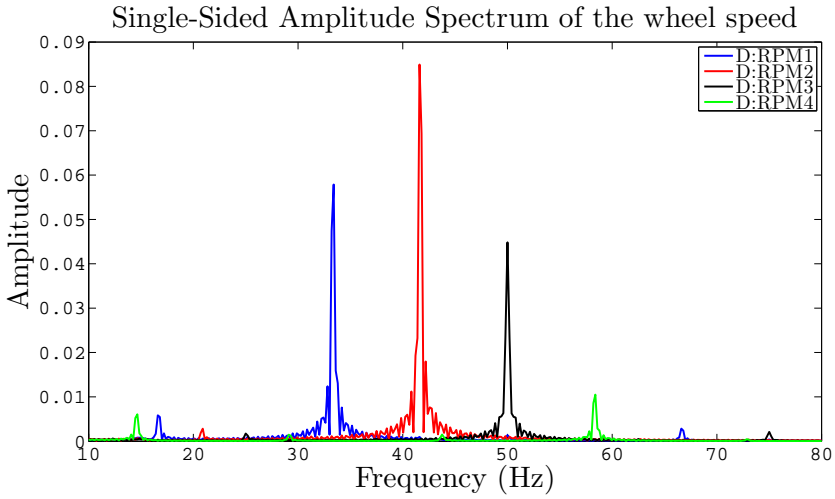


(a) Spectrum of the simulated wheel speed disturbances at D:RPM1, D:RPM2, D:RPM3 and D:RPM4 at gear four.

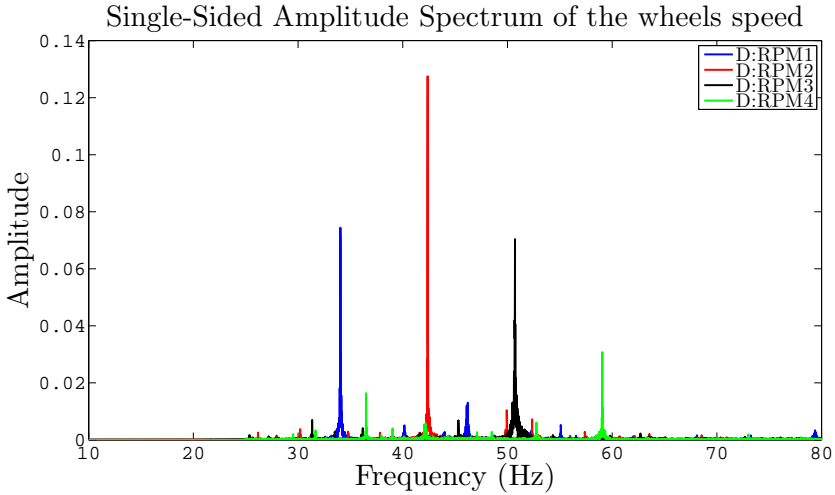


(b) Spectrum of the measured wheel speed disturbances at D:RPM1, D:RPM2, D:RPM3 and D:RPM4 at gear four.

Figure 5.8. Comparison between the model output wheel speed disturbance and the wheel speed disturbance on a real car for gear four.

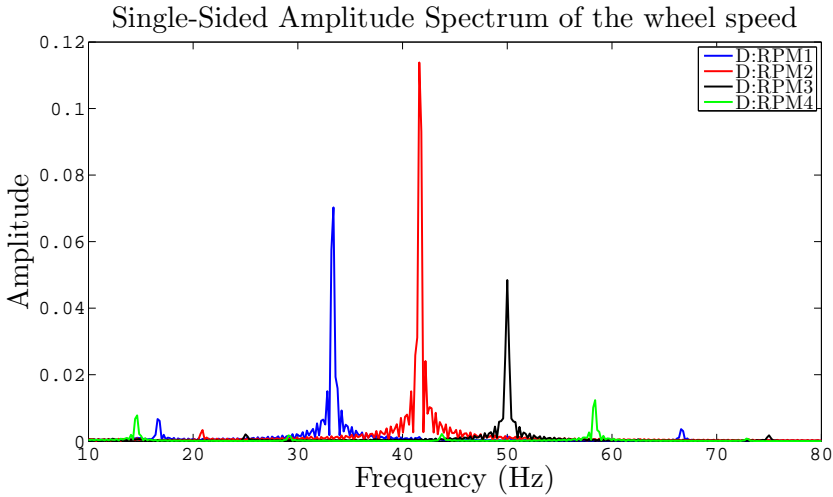


(a) Spectrum of the simulated wheel speed disturbances at D:RPM1, D:RPM2, D:RPM3 and D:RPM4 at gear five.

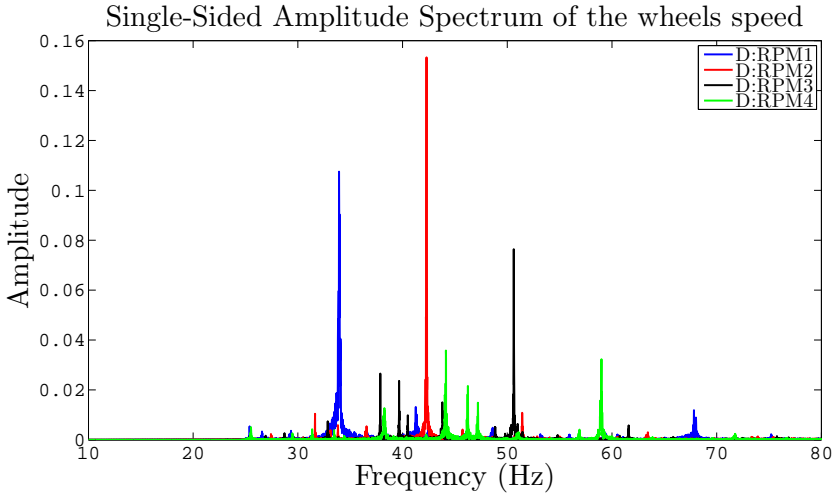


(b) Spectrum of the measured wheel speed disturbances at D:RPM1, D:RPM2, D:RPM3 and D:RPM4 at gear five.

Figure 5.9. Comparison between the model output wheel speed disturbance and the wheel speed disturbance on a real car for gear five.



(a) Spectrum of the simulated wheel speed disturbances at D:RPM1, D:RPM2, D:RPM3 and D:RPM4 at gear six.



(b) Spectrum of the measured wheel speed disturbances at D:RPM1, D:RPM2, D:RPM3 and D:RPM4 at gear six.

Figure 5.10. Comparison between the model output wheel speed disturbance and the wheel speed disturbance on a real car for gear six.

As it can be seen in the figures the frequencies of the disturbances in the model and the real car shows great correlation. The amplitude of the disturbances do not mach perfectly but the same characteristics can be seen in the simulation and the real car, the amplitude rises with higher gears and they both have a peak amplitude at D:RPM2 . Taking into account the error analysis discussed in the next section the general behavior of the model shows good resembles to the real car.

5.3.1 Error analysis

- Even though the geometrical parameters of the real engine and the ones in the model are the same there are other parameters that are virtually impossible to know the exact value of. This involves for example the intake manifold pressure p_{im} , the crankshaft angle at which the combustion starts θ_{SOC} and the polytropic constant for the expansion and compression, k_e and k_c . These parameters are not chosen at random but are well motivated in the literature, primarily [10].
- The driveline parameters are taken from [20] and are not identical to the ones in the car used for measurements. The good results however indicate that the parameters are valid and should be relatively close to the real cars parameters. The reason for not using the actual parameters of the car is that it is difficult to obtain such information.
- In [17] the original two wheel driveline, see Section 4.2 was implemented and the differential equations were solved using different solving methods. Figure 5.3 in her thesis shows how different solving methods results in different resulting amplitudes.
- In [8] different techniques for spectrum estimation are presented. It is shown that different spectral estimation strategies differ in the resulting amplitude whilst the actual frequency is an easier task to handle.

Chapter 6

Results and conclusions

6.1 Results

6.1.1 Natural frequencies

In Section 5.1.3, Test3b is described and it was conducted in order to locate potential natural frequencies in the driveline. During this test two sweeps were made in RPM with a diesel engine car and the result can be seen in Figures 6.1 to 6.4 which shows the empirical spectrum of the wheel speed on the rear and front tires for both sweeps. The spectrums were constructed by first removing the trends from the raw signal by using the *detrend* command in MATLAB. The MATLAB command *psd* was then used to create the empirical spectrums. In this chapter the specific engine speeds that were during the simulations process will not be spelled out at the request of NIRA Dynamics AB.

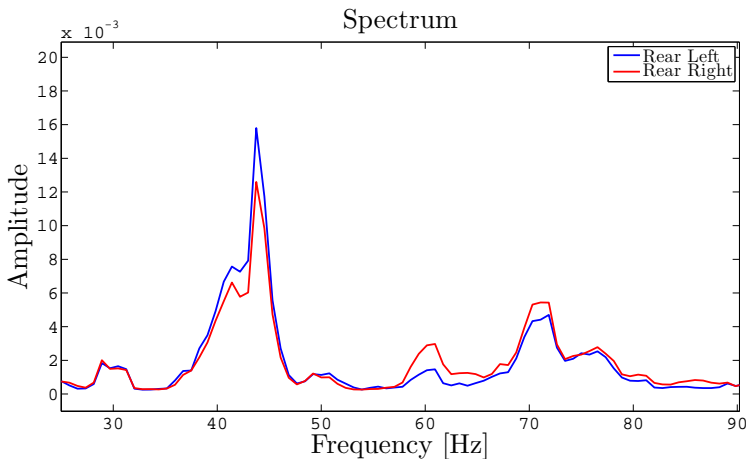


Figure 6.1. Spectrum of the rear wheel speed for the first sweep in Test3b.

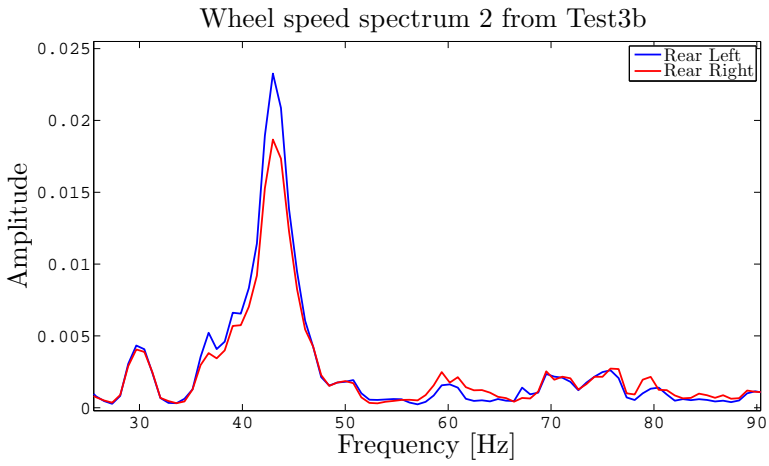


Figure 6.2. Spectrum of the rear wheel speed for the second sweep in Test3b.

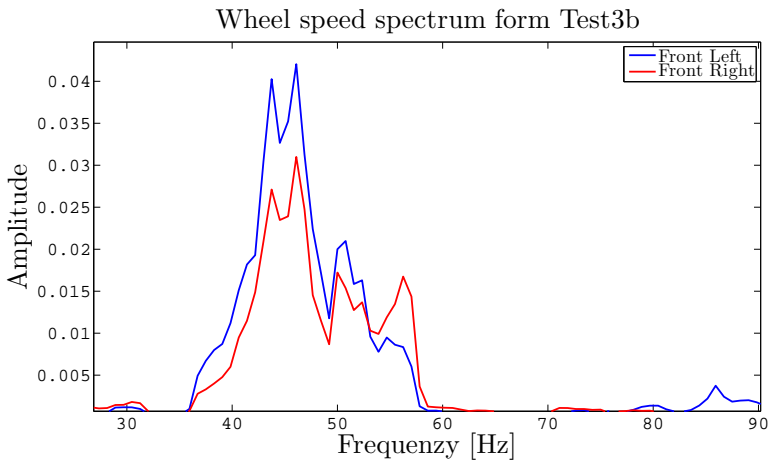


Figure 6.3. Spectrum of the front wheel speed for the first sweep in Test3b.

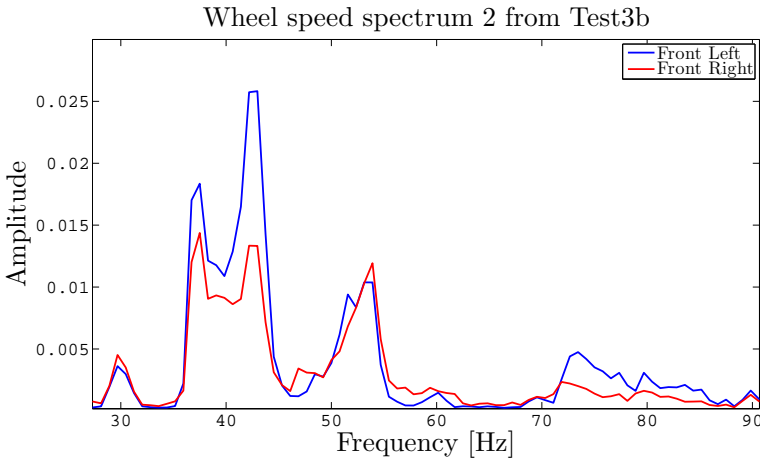


Figure 6.4. Spectrum of the front wheel speed for the second sweep in Test3b.

As can be seen in Figures 6.1 to 6.4 that there is a resonance peak at 43 Hz which indicates that a natural frequency is located at this frequency. This means that any frequency excited by the engine could be enhanced if it coincide with this natural frequency. In Figures 6.1.1-6.1.1 the wheel speed spectrums for two different cars with the same model and transmission, driving with engine speeds corresponding to sub frequencies (see Section 2.4) close to the natural frequency of 43 Hz. This is to illustrate how large effects resonance phenomena can have on the wheel speed disturbance.

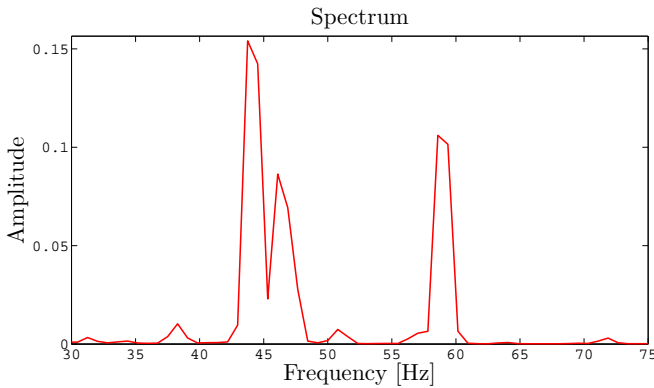


Figure 6.5. Spectrum of the front wheel speed for car one driving with an engine speed of 1750 RPM in the test rig at LiU. The main engine frequency can be calculated by Equation (2.1): $f_{main} = \frac{1750 \cdot 4}{60 \cdot 2} = 58,3$ Hz, which shows as the right peak in the spectrum. The larger peak at 43,75 Hz is however a result of a sub engine frequency exciting the natural frequency at 43 Hz. Equation (2.1) can be used here as well with $N = 3$: $f_{sub,3} = \frac{1750 \cdot 3}{60 \cdot 2} = 43,75$ Hz.

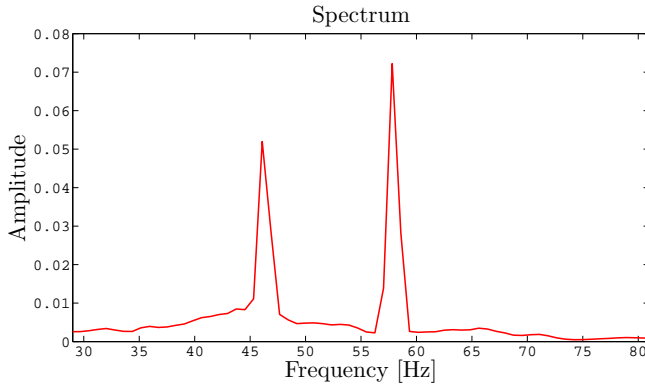


Figure 6.6. Spectrum of the rear wheel speed of car two driving with an engine speed of 1741 RPM on asphalt road. The main engine frequency is excited and shows as a peak at 57,8 Hz, the smaller peak at 46,1 Hz is however a result of a sub engine frequency exciting the natural frequency which now is a little bit higher than for car one, probably because car one did not have any tires mounted during the measurements.

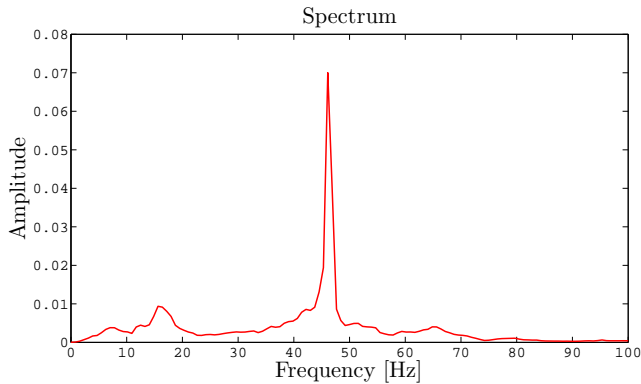


Figure 6.7. Spectrum of the rear wheel speed of car two driving with an engine speed of 2698 RPM on asphalt road. The disturbances from the main engine frequency 90 Hz is so small that it does not even show in the spectrum. A sub engine frequency however excites at the natural frequency and gives a large resonance peak at this frequency.

The resonance frequency of car two (the one driving on a road) at 46 Hz corresponds well to the natural frequency calculated for the four wheel drive model in Table 4.4.

The fact that the resonance peaks show on both the front and the rear wheel speeds indicate that the source of this natural frequency should be located somewhere before the differential gear dividing the torque between the front and rear axle.

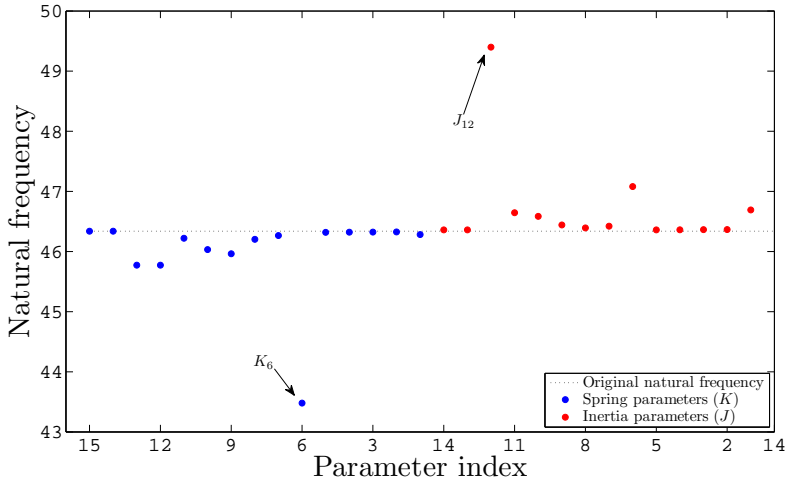


Figure 6.8. Sensitivity analysis of the sixth natural frequency in Table 4.4 in order to identify the parameters that mainly affect this frequency.

A sensitivity analysis where made in order to see which parameters in the model that control the 46 Hz natural frequency. In order to do this the inertia and stiffness parameters in the model where separately reduced with 20% and the sixth natural frequency (the sixth natural frequency is the one corresponding to 46 Hz, see Section 4.7) where calculated. The damping parameters where not included in the analysis since it is the undamped natural frequencies that are calculated. The result is shown in Figure 6.8 where it can be seen that the parameters k_6 and J_{12} (see Section 4.2) are the ones that mainly determines the position of the natural frequency. If one were to physically interpret these parameters they would correspond to the stiffness of the axis between the flywheel and the gearbox and the equivalent mass of the differential gears on the rear and the front axle. In order to see how the other natural frequencies depend on these parameters the same test where conducted again but none of them had its main dependency on these parameters. Another interesting observation from Figure 6.8 is that this particular natural frequency does not depend on neither the parameters related to the wheels or the engine, so a change of wheels and engine would not effect this natural frequency remarkably.

6.1.2 Engine dependency

There are certain engine specific properties that affect the wheel speed disturbance more than others. For example it is known that diesel engines generate more pronounced disturbances than petrol engines and one of the main differences between a petrol and a diesel engine is the compression ratio, see Section 3.3.7. Figure 6.9 shows the results from Test1 and Test2 disclosing the typical difference in disturbance amplitude for a petrol and diesel engine; Figure 6.10 shows the model wheel

speed difference for a diesel and petrol engine. The size of the flywheel has a direct effect on the wheel speed disturbance as well and as mentioned earlier its main purpose is to dampen the engines fluctuating torque. In this section the derived model will be used to examine how large effects changes in these parameters have on the wheel speed disturbances.

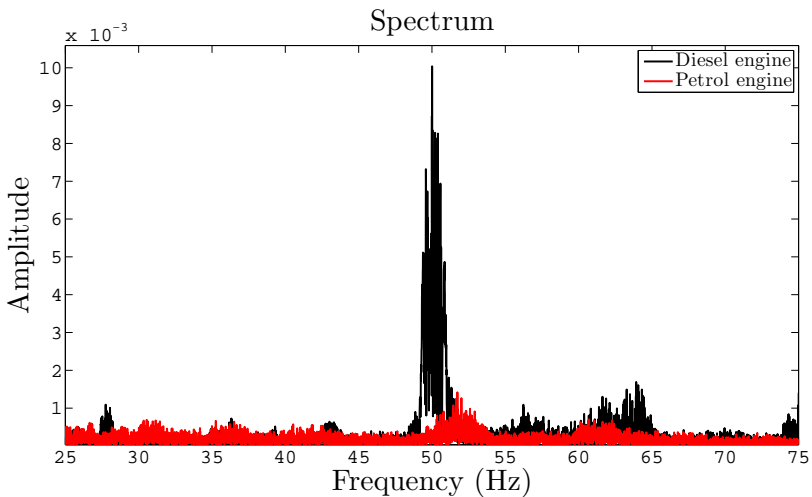


Figure 6.9. Spectrum of the wheel speed for a diesel car and a petrol car driving with engine speeds at T1:RPM3 and T2:RPM1. The data comes from Test1 and Test2 and one can see that the disturbance level is considerable smaller in the petrol car.

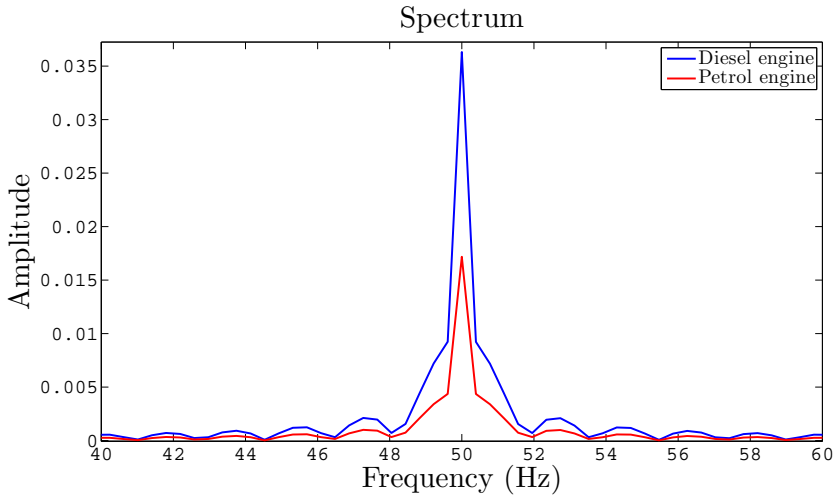


Figure 6.10. Spectrum of the simulated wheel speed for a diesel and petrol engine which shows smaller disturbance amplitude for the petrol engine compared to the diesel engine.

In order to examine the effect of the change in compression ratio the diesel and petrol engine models were parameterised with the same geometrical engine parameters as the cars in Test1 and Test2, the parameters can be seen in Table 6.1 and 6.2.

Parameter	Value
Displacement	1968 cm^3
Bore	81 mm
Stroke	95,5 mm
Compression ratio	16,5:1

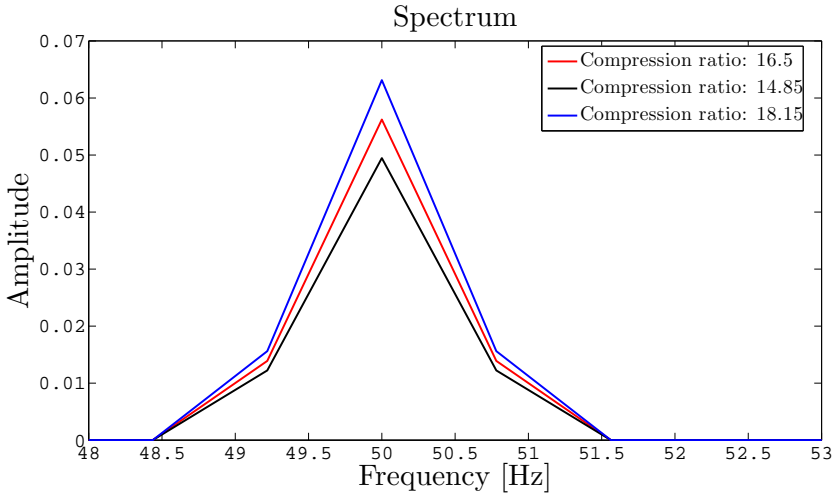
Table 6.1. Geometrical diesel engine parameters used for the simulation, [1].

Parameter	Value
Displacement	1984 cm^3
Bore	82,5 mm
Stroke	92,8 mm
Compression ratio	9,6:1

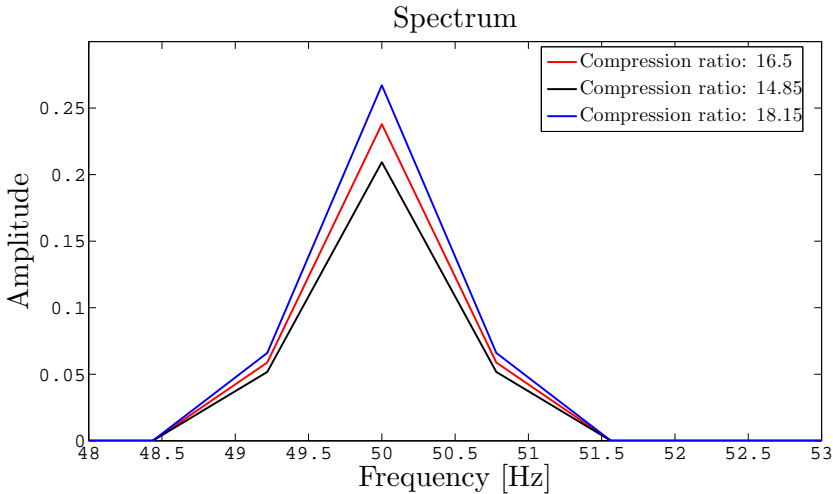
Table 6.2. Geometrical petrol engine parameters used for the simulation, [1].

The compression ratio of the engines were then changed with plus minus 10% and the result can be seen in Figure 6.11 to 6.12. The figures show the wheel speed

spectrum for an engine speed of CR:RPM and one can see that a 10% change in the compression ratio gives approximately 12% change in the amplitude. It should be noted that this only illustrates the change in compression ratio and do not take in to consideration the thermal properties in the engine that is difficult to know and will probably change with the compression ratio.

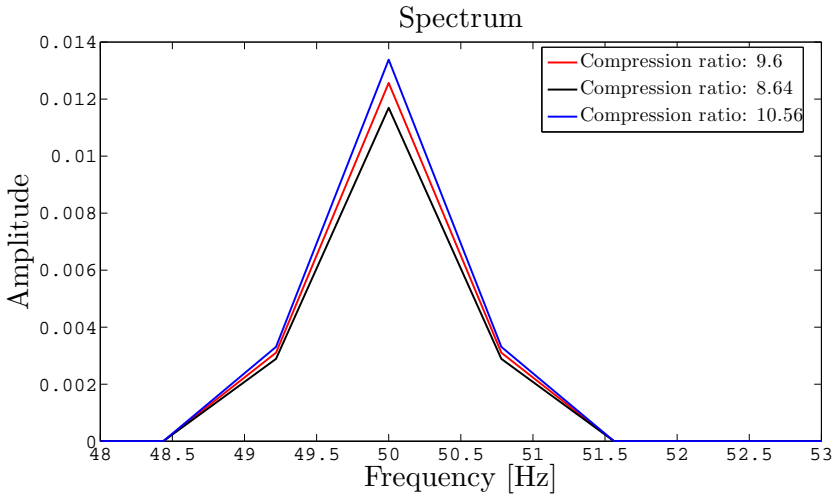


(a) Spectrum of the simulated front wheel speed which illustrates the change in disturbance amplitude for a diesel engine car with varying compression ratio.

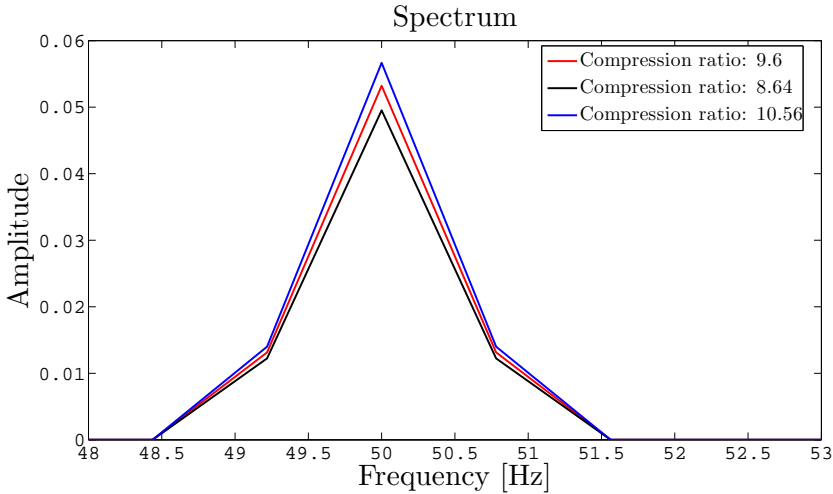


(b) Spectrum of the simulated rear wheel speed which illustrates the change in disturbance amplitude for a diesel engine car with varying compression ratio.

Figure 6.11. Illustration of the effect of compression ratio changes on the wheel speed disturbance.



(a) Spectrum of the simulated front wheel speed which illustrates the change in disturbance amplitude for a petrol engine car with varying compression ratio.

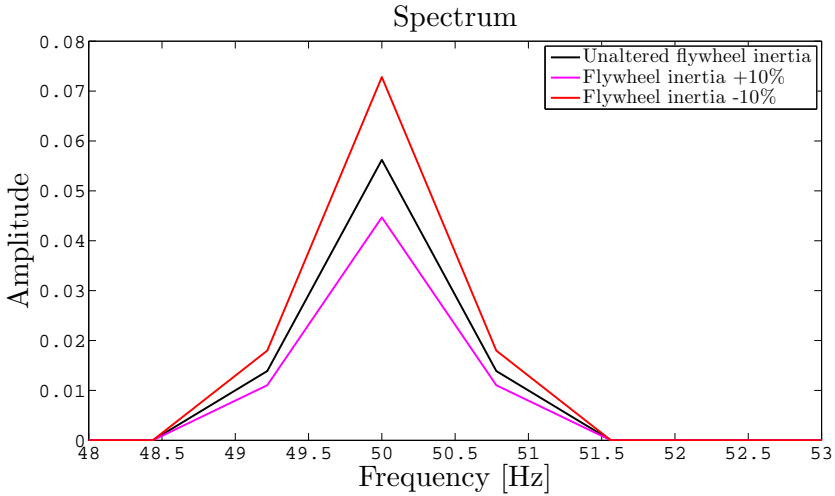


(b) Spectrum of the simulated rear wheel speed which illustrates the change in disturbance amplitude for a petrol engine car with varying compression ratio.

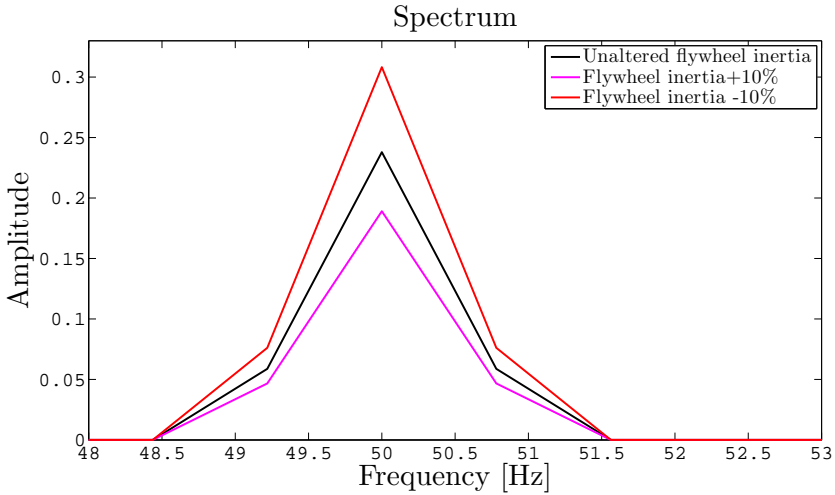
Figure 6.12. Illustration of the effect of compression ratio changes on the wheel speed disturbance.

The examination of the effect of the flywheel inertia where done in similar way as the compression ratio test. In this case however the engine parameters are kept constant according to Table 6.1 and the flywheel inertia was changed with plus minus 10%. Figure 6.13 shows the resulting difference in disturbance amplitude for an engine speed of FW:RPM . It can be seen that the 10% change in the flywheel inertia results in up to 30% change in the disturbance amplitude, this is three times the change when a change in compression rate where done.

It can be concluded that the wheel speed disturbances are more sensitive to changes in flywheel inertia than for a different compression ratio.



(a) Spectrum of the simulated front wheel speed which illustrates the change in disturbance amplitude for a diesel engine car with varying flywheel inertia.



(b) Spectrum of the simulated rear wheel speed which illustrates the change in disturbance amplitude for a diesel engine car with varying flywheel inertia.

Figure 6.13. Illustration of the effect of flywheel inertia changes on the wheel speed disturbance.

6.1.3 Front vs. rear wheel disturbances

When the wheel speed disturbances are investigated in the database available at NIRA Dynamics AB it can be seen that for four wheel driven cars the disturbance

amplitude on the front wheels are smaller than for the rear wheels. In Section 4.4 a way to parameterise the front and rear wheel propeller shaft were presented. The idea is that the front propeller shaft is both lighter and stiffer than the rear propeller shaft. When this parameterisation is used in the model for simulations at engine speeds FW:RPM1, FW:RPM2 and FW:RPM3 and $x = 0,28$ (see Section 4.4) one can see that the disturbance amplitude on the front wheels are considerable smaller comared to the rear wheels. The results are illustrated in Figure 6.14. This indicate that one of the main reasons for the difference in disturbance amplitude on the rear and front wheels are the one presented in Section 4.4.

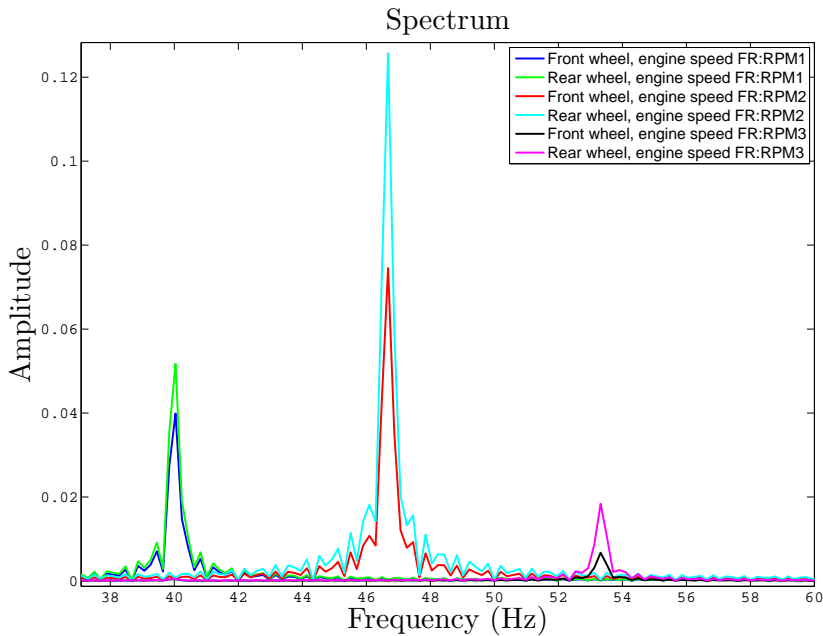


Figure 6.14. Simulated wheel speed spectrum for the front and rear wheels of a car driving in FW:RPM1, FW:RPM2 and FW:RPM3.

Chapter 7

Conclusions

A model of a powertrain which describes the wheel speed disturbances in a passenger car has been derived and validated. The model is general in the sense that it can describe both diesel and petrol engines, it can describe a two wheel driven car as well as a four wheel driven car and it can with slight changes describe the behavior of an engine with an arbitrary number of cylinders. The parameters in the model have a physical meaning and can therefore be changed into corresponding parameters of a specific engine and driveline. These parameters are however hard to obtain and generic parameters are presented so that the model can be used without the exact numbers. This could prove useful in the early stages of a project in which the model would be used.

When the model was used to gain knowledge of how different physical aspects of the engine and driveline affect the wheel speed disturbance, one could see how large effects the natural frequencies have on the wheel speed disturbance and how these frequencies can be excited by sub frequencies in the engine fluctuations. It was also visualised how large effect the mass of the flywheel and the compression ratio of the engine have when it comes to the wheel speed disturbances. It could also be concluded through the reasoning of this thesis that one of the main reasons of the difference in disturbance amplitude of the front and the rear wheels in a four wheel driven car is the difference in the driveline geometrics in the front and rear systems of a car. More specific the fact that the axles in the front of the car often are both lighter and stiffer than in the rear axles.

The algorithm presented in the thesis for calculation of the frequency in which the powertrain disturbances could be expected is proven to be useful for an arbitrary number of cylinders. The algorithm can therefore be used in cars with so called cylinder shutdown capability. When it comes to the use of this work for NIRA Dynamics AB the presented results will be able to improve the search pattern which TPI uses to search for engine and driveline related disturbances. This thesis will also contribute to increased knowledge of powertrain related disturbances and its sources.

7.1 Future work

In this section different subjects that may be considered as future work for this master thesis will be presented. One of the biggest issues when using this model is that it has a relatively long simulation time, but this could be rectified by reducing the complexity of the model and thereby the simulation time. Therefore the model could be implemented in real-time use e.g. in the disturbance suppression algorithm in TPI. Another direction of future work could be to expand the model by including some of the non-linear components of the driveline such as the universal joints in the propeller shaft. This would however increase the simulation time. If the model should to be used in the same manner as in this thesis; investigating the effects and finding the root causes of the wheel speed disturbance, it could be expanded to increase flexibility. Ability to easier choose the number of cylinder of the engine and the number of active cylinder and so on. This would not necessarily have to increase the computation time.

Bibliography

- [1] <http://www.automobile-catalog.com/>. April 2012.
- [2] H Bartlett A. Farshidianfar, M Ebrahimi. Hybrid modelling and simulation of the torsional vibration of vehicle driveline systems. 2001.
- [3] J. Park Y. Son B. Lim, I. Lim. Estimation of the Cylinder Pressure in a SI Engine Using the Variation of Crankshaft Speed. (SAE Technical paper No. 940145), 1994.
- [4] D. Crolla B. Mashadi. *Vehicle Powertrain Systems*. WILEY, 2012.
- [5] J. Scarpati et al. Prediction of Engine Noise using Parameterized Combustion Pressure Curves. *SAE International*, 2007.
- [6] N. Persson F. Gustavsson. Virtual sensors of tire pressure and road friction. In *Society of Automotive Engineers World Congress, Detroit, MI, USA*, number SAE 2001-01-0796, Mar 2001.
- [7] C. Jezek F. Jones. Diesel combustion modeling and simulation for torque estimation and parameter optimization. Master's thesis Master's thesis LiTH-ISY-08/4072-SE, Department of Electrical Engineering, Linköping University, 2008.
- [8] Monson H. Hayes. *Statistical Digital Signal Processing and Modeling*. WILEY, 1996.
- [9] I. Dincer J. Nieminen, N. D'Souza. Comparative combustion characteristics of gasoline and hydrogen fuelled ICEs. *International journal of hydrogen energy*, 2000.
- [10] I. Andersson L. Eriksson. An Analytic Model for Cylinder Pressure in a Four Stroke SI Engine. *SI engine modeling, Detroit, MI, USA*, 2002.
- [11] L. Nielsen L. Eriksson. *Modeling and Control of Engines and Drivelines*. Vehicular Systems, ISY Linkopings Institute of Technology, 2009.
- [12] T. Glad L. Ljung. *Modellbygge och simulering*. Studentlitteratur, 2009.
- [13] Lars Nielsen Magnus Petterson. Diesel engine control with handling of driveline reconances. *Control engineering practice*, 2002.

-
- [14] J. Malm. Cylinder-by-cylinder torque model of an a SI-engine for real-time applications. ISRN LUTFD2/TFRT-5772-SE, Department of Electrical Engineering, Linköping University, Linköping, Sweden, December 2005.
- [15] M. Drevo N. Persson, F. Gustavsson. Indirect tire pressure monitoring using sensor fusion. Technical Report LiTH-ISY-R-2471, Department of Electrical Engineering, Linköping University, SE-581 83 Linköping, Sweden, Oct 2002.
- [16] M. H. Nayeri. All wheel drive hardware dependant control. Master's thesis Master's thesis LiTH-ISY-05/3830-SE, Department of Automatic Control, Lund Institute of technology, 2006.
- [17] N. Nickmehr. Ride quality and drivability of a typical passenger car subject to engine/driveline and road non-uniformities excitations. Master's thesis LiTH-ISY-11/4477-SE, Department of Electrical Engineering, Linköping University, Linköping, Sweden, 2011.
- [18] N. Persson. Estimation properties of a tire pressure monitoring system. Technical Report LiTH-ISY-R-2472, Department of Electrical Engineering, Linköping University, SE-581 83 Linköping, Sweden, Oct 2002.
- [19] J. Gundersen R. Bengtsson. Truck differential and rear axle modeling. Master's thesis, Department of Automatic Control, Lund University, Lund, Sweden, May 2010.
- [20] El-Adl Mohammed Aly Rabeih. *Torsional Vibration Analysis of Automotive Driveline*. PhD thesis, Mechanical Engineering Department, the university of Leeds, 1997.

Appendix A

Notation

A.1 Variables and parameters

The parameters and variables that are used in the thesis can be seen below in order of appearance.

Table A.1: Parameter and variable list.

Variable	Description
f_{main}	Main engine frequency
N	Number of cylinders
RPM	Rounds per minute
p_c	The compression pressure
p_{ivc}	The pressure in the cylinder when the intake valve is closed
V_{ivc}	The cylinder volume when the intake valve is closed
k_c	Polytropic constant for the compression
$V(\theta)$	Cylinder volume as a function of crank angle
T_c	The temperature inside the cylinder during the compression
T_{ivc}	Temperature inside the cylinder when the intake valve is closed
p_{im}	Intake manifold pressure
T_{af}	Air-fuel mixture temperature
T_r	Residual gas temperature
x_r	Residual gas fraction
p_e	The expansion pressure
p_3	Cylinder pressure in state three in the Otto-cycle
V_3	Cylinder volume in state three in the Otto-cycle
k_e	Polytropic constant for the expansion
T_e	The expansion temperature
T_3	Temperature in the cylinder in state three in the Otto-cycle
T_2	Temperature in the cylinder in state two in the Otto-cycle
T_{comb}	temperature increase due to the combustion
m_f	Fuel mass

Table A.1: (Continued)

Variable	Description
$q_H V$	Fuel heating value
$\eta_f(\lambda)$	Fuel conversion efficiency
c_v	Specific heat constant at constant volume
m_{tot}	Total mass of the fuel, air and residual gases
$\lambda(A/F)_s$	The stoichiometric air-fuel ratio
p_2	Cylinder pressure in state two in the Otto-cycle
x_b	Percentage of burned fuel
$\Delta\theta_d$	Flame development angle
$\Delta\theta_b$	Rapid burn angle
$\Delta\theta_d$	Combustion duration angle
θ_c	Combustion angle
$mf b_{50}$	Point where 50% of the fuel mass is burned
$MF B_{50,OPT}$	The optimal point at which 50% of the fuel mass is burned
ϵ	Compression ratio
V_{max}	The cylinders maximum volume
V_{min}	The cylinders minimum volume
F_{cr}	The force applied on the crankshaft on the piston
P_g	The gas pressure inside the cylinder
A_p	Piston top area
F_t	The force from the piston that are orthogonal to the crankshaft
θ	Crankshaft angle
T_g	The resulting torque on the crankshaft
R	Crankshaft radius
M	Mass moment of inertia matrix
C	Torsional damping matrix
K	Stiffness matrix
F	Applied force matrix
x	Position vector
k_i	Denotes the stiffness of spring i
c_i	Denotes the damping of damper i
J_i	Denotes the mass moment of inertia of body i
J_T	Second moment of area
G	Modulus of rigidity
F_t	Tractive force
m	Car mass
v	Car longitudinal velocity
c_w	Air resistance constant
A_a	Frontal area of the car
ρ_a	Air density
c_r	Rolling resistance constant
g	Current planets gravitational constant
α	Road angle
s	Slip factor

Table A.1: (Continued)

Variable	Description
r_0	Effective wheel radius
ω	Wheel angular speed
$F_{w,i}$	Applied force on tire i
C_x	The effective longitudinal stiffness of the tire
$T_{w,i}$	Applied torque on tire i

A.2 Acronyms

TPI	Tire Pressure Indicator
TPMS	Tire Pressure Monitoring System
iTPMS	indirect Tire Pressure Monitoring System
dTPMS	direct Tire Pressure Monitoring System
DAE	Differential Algebraic Equations
SI	Spark Ignited
TDC	Top Dead Center
BDC	Bottom Dead Center
ICE	Internal Combustion Engine
IVO	Intake Valve Opening
EOC	End of Combustion
IVC	Intake Valve Closing
SOC	Start of Combustion
EVO	Exhaust Valve Opening
EVC	Exhaust Valve Closing
RPM	Rounds Per Minute

Appendix B

Cylinder volume

In this section an expression for the cylinder volume as a function of the crank angle θ is derived. In Figure B.1 an illustration of a cylinder and its components are shown.

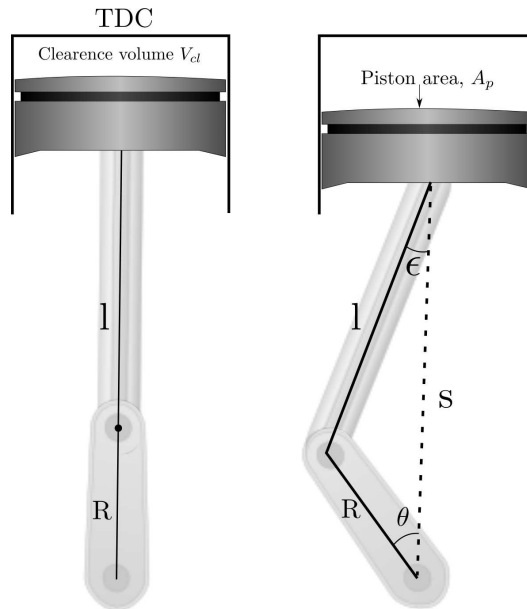


Figure B.1. Describes the geometric properties of a cylinder

The cylinder volume, $V(\theta)$ are given as:

$$V(\theta) = V_{cl} + (l + R - s(\theta))A_p \quad (\text{B.1})$$

$$s(\theta) = R \cos(\theta) + l \cos(\epsilon) \quad (\text{B.2})$$

Where l is the connecting rod length, R is the crankshaft radius, V_{cl} is the cylinder clearance volume, A_p is the piston area, s is the length from the crankshaft center to the piston and θ is the crankshaft angle. The angle ϵ is unknown and $\cos(\epsilon)$ are given by the well know law of cosine:

$$\cos(\epsilon) = \frac{s^2 + l^2 - R^2}{2sl} \quad (\text{B.3})$$

Equations (B.2) and (B.3) gives:

$$s(\theta) = R \cos(\theta) + \frac{s^2 + l^2 - R^2}{2s} \Rightarrow s(\theta)^2 - 2sR \cos(\theta) - (l^2 - R^2) = 0 \quad (\text{B.4})$$

When the positive solution of (B.4) are put in to (B.1) the final expression for the cylinder volume are obtained

$$V(\theta) = V_{cl} + (l + R - R \cos(\theta) - \sqrt{l^2 - R^2 - R^2 \cos(\theta)^2}) A_p \quad (\text{B.5})$$